nature communications

Article

https://doi.org/10.1038/s41467-024-51041-1

Circular RNAs regulate neuron size and migration of midbrain dopamine neurons during development

Received: 4 May 2023

Accepted: 26 July 2024

Published online: 08 August 2024

Check for updates

Mateja Rybiczka-Tešulov[1,4], Oxana Garritsen[1], Morten T. Venø[2,3], Laura Wieg[1], Roland van Dijk[1,5], Karim Rahimi[2,6], Andreia Gomes-Duarte[1,5], Marina de Wit[1], Lieke L. van de Haar[1,7], Lars Michels[1,5], Nicky C. H. van Kronenburg[1], Christiaan van der Meer[1], Jørgen Kjems[2], Vamshidhar R. Vangoor[1] & R. Jeroen Pasterkamp[1]

Midbrain dopamine (mDA) neurons play an essential role in cognitive and motor behaviours and are linked to different brain disorders. However, the molecular mechanisms underlying their development, and in particular the role of non-coding RNAs (ncRNAs), remain incompletely understood. Here, we establish the transcriptomic landscape and alternative splicing patterns of circular RNAs (circRNAs) at key developmental timepoints in mouse mDA neurons in vivo using fluorescence-activated cell sorting followed by short- and long-read RNA sequencing. In situ hybridisation shows expression of several circRNAs during early mDA neuron development and post-transcriptional silencing unveils roles for different circRNAs in regulating mDA neuron morphology. Finally, *in utero* electroporation and time-lapse imaging implicate circ*Rmst*, a circRNA with widespread morphological effects, in the migration of developing mDA neurons in vivo. Together, these data for the first time suggest a functional role for circRNAs in developing mDA neurons and characterise poorly defined aspects of mDA neuron development.

The midbrain dopamine (mDA) system modulates cognitive processes, regulates voluntary movement and mediates responses to rewarding and aversive stimuli. It is anatomically subdivided into the substantia nigra pars compacta (SNc), ventral tegmental area (VTA) and retrorubral field (RRF), but further subdivisions have been made on basis of molecular signatures, connectivity patterns and function[1]. mDA neurons send efferent projections through the mesostriatal and mesocorticolimbic pathways to select areas in the forebrain and have been linked to various brain disorders, including addiction, schizophrenia and Parkinson's disease (PD)[2]. During development, mDA neurons differentiate from progenitors in the midbrain ventricular zone to subsequently migrate into the ventral midbrain (vMB). Here, they develop efferent axonal projections and complex dendritic trees. For a comprehensive overview of mDA neuron development and physiology, see reviews[1,3–5]. While initial stages of mDA neuron development, such as cell fate specification and differentiation, have been characterised in detail, much less is known about subsequent developmental processes, including regulation of neuronal morphology and neuron migration.

[1]Department of Translational Neuroscience, UMC Utrecht Brain Center Utrecht, University Medical Center Utrecht, Utrecht University, Utrecht, The Netherlands. [2]Department of Molecular Biology and Genetics, Interdisciplinary Nanoscience Centre, Aarhus University, Aarhus C, Denmark. [3]Omiics ApS, Aarhus N, Denmark. [4]Present address: Institute of Medical Genetics, Center for Pathobiochemistry and Genetics, Medical University of Vienna, Vienna, Austria. [5]Present address: VectorY Therapeutics, Matrix Innovation Center VI, Amsterdam, The Netherlands. [6]Present address: Department of Genetics, Blavatnik Institute, Harvard Medical School, MA Boston, USA. [7]Present address: Berlin Institute for Medical Systems Biology, Max Delbrück Center, Berlin, Germany. e-mail: r.j.pasterkamp@umcutrecht.nl

The formation of functional mDA neurons requires cooperation between a plethora of molecular factors, including transcription factors, chemokines, axon guidance cues and cell adhesion molecules. For example, migration of embryonic mouse mDA neurons is in part regulated by chemokine CXC-motif ligand 12 (CXCL12) and the extracellular matrix component reelin (RELN), while soma positioning in the SNc requires the axon guidance cue NETRIN-1[6–10]. To gain more insight into the molecular regulation of mDA neuron-related cellular processes, several studies have performed transcriptomic profiling of mDA neurons[11–15]. Most of this work is focused on coding genes, with few exceptions (e.g[16].). However, in addition to mRNAs and their protein products, non-coding RNAs (ncRNAs) have been implicated in the regulation of key developmental events in neurons (e.g[17–19].). It is estimated that less than 2% of the human genome encodes protein, while most nucleotides are transcribed into RNA thus giving rise to an exquisitely high number of ncRNAs. NcRNAs longer than 200 nucleotides are defined as long ncRNAs, and both linear and circular long ncRNAs exist (referred to here as lncRNAs and circRNAs, respectively)[20,21]. Interestingly, lncRNAs and circRNAs have been implicated in PD[22–25] and were studied in embryonic midbrain neurons[26,27], but their expression, regulation and function during mDA neuron development remain largely unexplored.

Compared to other classes of ncRNAs, our understanding of the role and mechanism-of-action of circRNAs is rather rudimentary and processes such as circRNA biogenesis and evolutionary origin are actively investigated[20,28]. CircRNAs form as result of backsplicing, a process introducing a covalent bond between 5′- and 3′-splice sites in a pre-mRNA molecule[29–32]. Expression of circRNAs is temporally regulated, tissue- and cell type-specific and particularly high in the brain[26,30,33,34]. Further, circRNAs are enriched in specific subcellular neuronal compartments and dysregulated in brain diseases[24,33–35]. Interestingly, two recent studies functionally implicate circRNAs in neural development by showing roles for circ*SLC45a4* and circ*Fat3* in neural progenitor differentiation and cell positioning in the mouse cortex[36,37]. However, although thousands of circRNAs are expressed in brain tissue, their role in neurons in vivo remains mainly unknown.

In this study, we define the expression patterns and potential cellular roles of circRNAs in developing mDA neurons. First, immunohistochemistry was used in combination with genetic mouse models to gain a more comprehensive understanding of mDA neuron development. Short-read RNA sequencing (RNAseq) and circRNA long-read sequencing (LRS) were then performed to establish the expression profiles (circRNA abundance) and alternative splicing (AS) patterns of circRNAs in mDA neurons at key developmental timepoints. This revealed mDA neuron- and developmental stage-specific patterns of circRNA expression levels and alternative splicing. Single-molecule fluorescence in situ hybridisation (smFISH) was used study the distribution of circRNAs in mDA neurons in vitro and in vivo. And finally, knockdown (KD) of selected circRNAs (circ*Ezh2*, circ*Fat3*, circ*Rmst* and circ*Tulp4)* suggested a role for circRNAs in the regulation of different aspects of mDA neuron morphology and tyrosine hydroxylase-positive (TH^+) neuron number in vitro. Experimental reduction of the abundance of one of the candidates, circ*Rmst*, in organotypic slices or in vivo caused an acceleration of neuron migration and lateral mislocalization in the mDA neuron pool, respectively. Together, these data implicate circRNAs in mDA neuron development, further characterise poorly understood developmental processes in mDA neurons, and provide a framework for future studies into the role and regulation of circRNAs in the developing mDA system.

Results

Spatiotemporal analysis of mDA neuron development

In this study, we examined the function of circRNAs in mDA neuron development by transcriptomic profiling and functional analysis (Fig. 1a). Some aspects of mDA neuron development have been described in detail, whereas others remain less well understood (e.g. neuron migration, dendrite development). Therefore, to gain a more comprehensive understanding of mDA development, we first performed immunohistochemistry at specific developmental stages, in part combined with whole-brain clearing and fluorescent light sheet microscopy (FLSM) (Fig. 1a–c, Supplementary Fig. 1). TH was used to label mDA neurons. However, the high density of mDA neurons in the midbrain often complicated their analysis at the cellular level. Therefore, *Pitx3-ITC;ACTB-Flp* mice, in which SNc mDA neurons are labelled more sparsely[10], were used (Fig. 1b, Supplementary Fig. 1) for a more detailed examination of for example the migration and dendritic development of (ventral) SNc neurons.

$Citrine^+$ SNc neurons were first detected at embryonic day (E)13, had an elongated shape and positioned their somata ventrolaterally at E14, following the completion of tangential migration. Already during their migration, mDA neurons extended neurites and TH-positive (TH^+) axons were found projecting towards the habenula and striatum as early as E12 (Fig. 1b, c, Supplementary Fig. 1). In consecutive days, axons fasciculated into larger bundles and dendritic outgrowth occurred, both within the SNc and the substantia nigra pars reticulata (SNr). As development progressed, dendrites in the rostral SNr fasciculated into so-called 'dendrons'[38]. A few TH^+ neurons were detected in the SNr along the ventral edge of the SNc (Fig. 1b, Supplementary Fig. 1). We then used these and other observations to complement previously published observations for generating a comprehensive timeline of cellular events comprising mDA neuron development (Fig. 1d). This overview was subsequently used for selecting developmental stages for the analysis of circRNAs.

Expression of circRNAs in embryonic mDA neurons

For the mDA system, E14 appeared to be a time point at which many cellular events occur, including mDA neuron specialisation, migration, axon extension and early neurite development (Fig. 1d). Therefore, this timepoint was selected to examine whether mDA neuron-enriched circRNAs exist. We combined fluorescence-activated cell sorting (FACS) and rRNA-depleted short-read RNAseq of cells from E14 *Pitx3-GFP* mouse ventral midbrains and first performed total RNA analysis as a control (Fig. 2a). In *Pitx3-GFP* mice, an eGFP expression cassette replaces exons 2, 3 and in part exon 4 of the *Pitx3* gene, allowing for specific labelling of PITX3-expressing mDA neurons[39]. Differential expression analysis (DESeq2[40]) of short-read total RNA demonstrated distinct RNA profiles for mDA neurons (774 genes enriched in GFP^+; padj < 0.05, l2fc > 1) and surrounding non-mDA cells (4711 genes enriched in GFP^-; padj < 0.05, l2fc < −1) (Supplementary Fig. 2a–d). The most highly abundant genes in the GFP^+ samples included classical mDA marker genes, e.g. *Th*, *Pitx3* and *Aldehyde dehydrogenase a1* (*Aldh1a1)* (Supplementary Dataset 1). In addition to RNA expression levels, alternative RNA splicing also impacts developmental processes[41]. Therefore, we determined alternative splicing (AS) patterns in mDA neurons by performing rMATS[42] analysis (Supplementary Fig. 2e–h, Supplementary Data 1). AS analysis of total RNAseq data revealed 847 AS events with a uniform distribution between enhanced and repressed splice junctions (FDR < 0.05, ΔPSI > 0.1; Supplementary Fig. 2f). Skipped exons (SE) comprised the largest category of differential AS events (578 events; Supplementary Fig. 2g). The other categories were mutually exclusive exon (46 events; MXE), alternative 5′splice site (34 events; A5′SS), alternative 3′splice site (71 events; A3′SS) and retained intron (118 events; RI). Together, these results validate the FACS-based RNAseq approach by demonstrating specific RNA expression profiles and differential AS patterns in embryonic mDA neurons.

Next, we examined circRNA levels in E14 mDA neurons using the validated RNAseq data. Despite the large number of neuronal circRNAs identified, their functional role in developing neurons remains rather poorly understood[33,34,36,37]. One way to minimise false-positive circRNA

https://doi.org/10.1038/s41467-024-51041-1

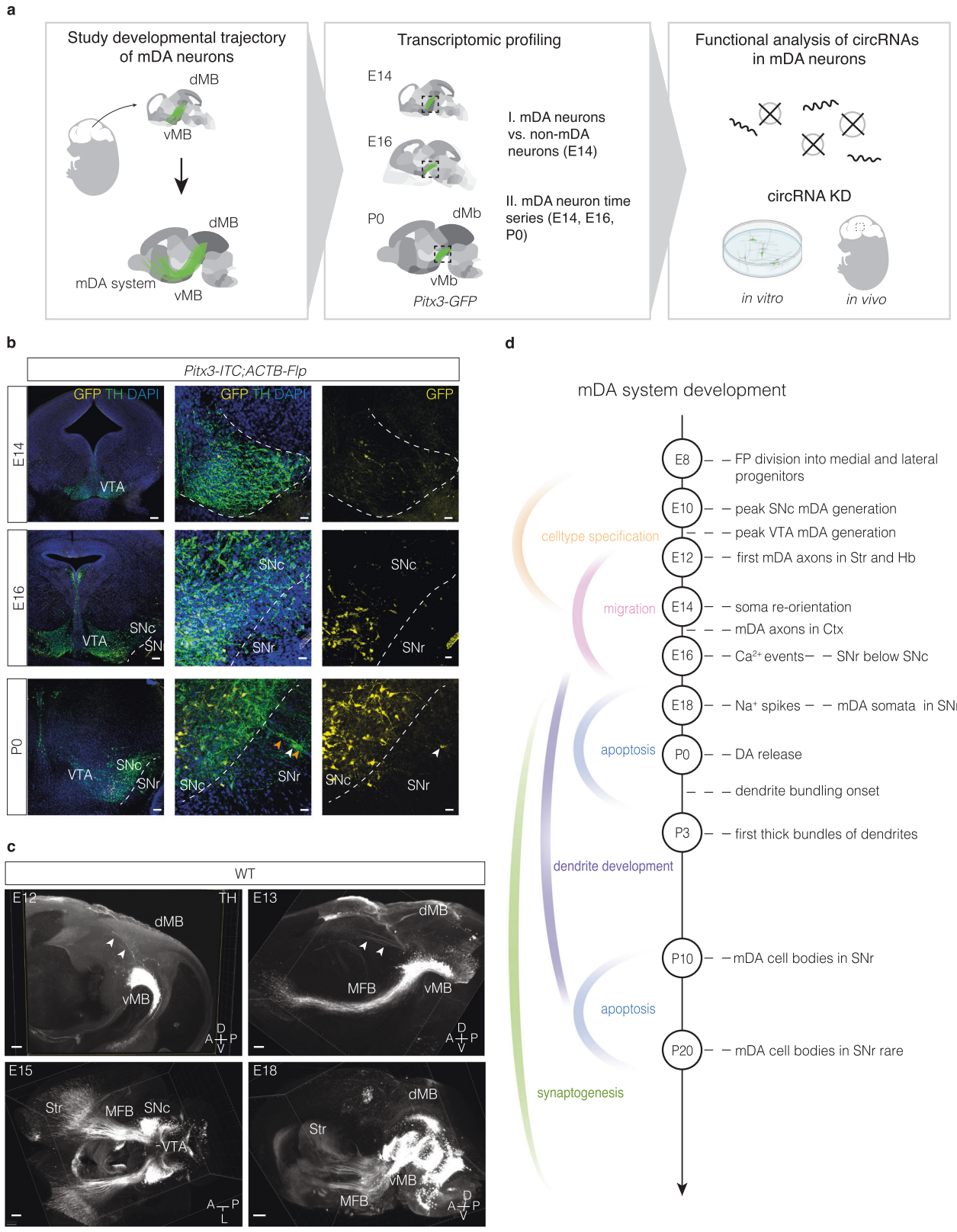

prediction, is to use a primary and a secondary tool for the annotation of BSJs[43]. A total of 3927 circRNAs were detected in the total embryonic RNA data using the tool find_circ[31] and 3354 of these were also detected using the additional prediction tool CIRCexplorer[44]. Based on the circRNA transcript profile (Fig. 2b), GFP$^+$ and GFP$^-$ samples grouped separately in PCA analysis (Supplementary Fig. 2i, Supplementary Data 1). Characterisation of all detected circRNAs revealed that they derived from all chromosomes and originated mostly from protein-coding host-genes. They consisted of 4.7 exons on average and the vast majority of transcripts in the dataset were linear, i.e. only few genes predominantly produced circRNAs (Fig. 2c–e, Supplementary Fig. 2j, Supplementary Data 1). Ten circRNAs were significantly enriched in mDA neurons (circ*Bnc2*, circ*Fat3*, circ*Gfra1*, circ*Gm21949*, circ*Lmx1a*, circ*Pbx1*, circ*Pbx3*, circ*AF529169*, circ*Pde5a* and circ*Rmst)*; (padj < 0.05,

Fig. 1 | Spatiotemporal analysis of mDA neuron development. a Experimental design of the study. Following analysis of the developmental trajectory of mDA neurons, transcriptomic profiling was performed to (I) compare mDA neurons (*Pitx3-GFP*+) and cells in their environment (GFP-) at E14, and (II) to determine RNA expression at several key developmental stages. Based on these observations circRNA expression and function were studied in more detail. **b** Immunohistochemistry of E14, E16 and P0 *Pitx3-ITC:ACTB-Flp* coronal vibratome sections. At P0, mDA dendrites reach into SNr. A few mDA neurons are present in the SNr (TH^+/ITC^- = orange arrow, TH^+/ITC^+ = white arrow). Dashed line indicates SNc/SNr boundary. Scale bars: column 1 = 100 μm, columns 2 and 3 = 20 μm. Representative images from n = 1. **c** Whole-mount immunostaining for TH followed by 3DISCO tissue clearing and FLSM of E12, E13, E15 and E18 WT brains. White arrows indicate TH^+ axons growing towards the Hb. Scale bars: E12 and E13 = 100 μm, E15 = 150 μm, E18 = 200 μm. Representative images from n = 1. **d** Schematic overview of key developmental events in mDA neuron development based on published literature and results from the present study. Key events include floorplate division[106], mDA neuron specification into SNc and VTA subsets[64], axon extension towards the forebrain[107], reorientation of mDA neuron axis during migration, formation of the SNr, first Ca^{2+} events, mDA neurons in SNr (visible until adolescence), fasciculation of mDA dendrites in SNr and formation of 'dendrons'[38], first Na^+ spikes[45], first DA release into the striatum[45] and apoptotic waves (around P0 and between P15 and P20)[108]. Ctx Cortex, dMb dorsal Midbrain, E embryonic day, mDA midbrain dopamine, MFB medial forebrain bundle, P postnatal day, SNc Substantia nigra pars compacta, SNr Substantia nigra pars reticulata, Str Striatum; TH Tyrosine hydroxylase, vMB ventral Midbrain, VTA Ventral tegmental area. Embryo and cell dish icons were from BioRender.com.

l2fc > 0.5) and one was expressed at significantly lower levels (circ*Plce1*) (padj < 0.05, l2fc < −0.5; Fig. 2f). Interestingly, several of these circRNAs derived from mDA neuron-specific coding genes (e.g. *Pbx1* and *Lmx1a*) or non-coding loci (lncRNA *Rmst*). Other circRNAs represented more general, highly abundant circRNAs, such as circ*Fat3*. Reverse transcription followed by quantitative PCR (RT-qPCR) with divergent primers amplifying the predicted backsplice junction (BSJ) further confirmed the existence of the predicted circRNAs circ*Bnc2*, circ*Epha5*, circ*Fat3*, circ*Gfra1*, circ*Lmx1a*, circ*AF529169*, circ*Pde5a*, circ*Rmst* and circ*Robo1* and circ*Plce1* in an independent sample of FACS-purified E14 mDA neurons (Fig. 2g).

Thus, embryonic mDA neurons display specific patterns of circRNA expression, several of which are generated from genes with important physiological roles in mDA neuron development.

Temporal dynamics of gene expression and regulation in developing mDA neurons

After having established that mDA neurons express specific circRNAs, we assessed whether their expression levels and regulation can be correlated with specific developmental stages. E14, E16 and P0 were selected as at these stages key developmental events occur, such as dendritic outgrowth, first spontaneous electrical activity and first DA release (Fig. 1d)[45]. First, rRNA-depleted short-read RNAseq analysis of total RNA from FACS-purified *Pitx3-GFP* (mDA) neurons was performed to validate the approach (timeseries dataset, Fig. 3a; Supplementary Data 2). This showed sample clustering according to developmental stage (Supplementary Fig. 3a, b; Supplementary Data 2). Comparison of total RNA expression at E14 and E16, E16 and P0, and E14 and P0 yielded 247, 150 and 843 differentially expressed genes (DEGs, analysed using DESeq2, padj < 0.05, l2fc > 1 and l2fc < −1). Next, to gain insight into the temporal dynamics of AS during mDA neuron development, differential exon usage[46] (DEU) was assessed which revealed 140 exons with statistically significant DEU from total RNA. Comparison of E16 and E14, P0 and E16, and P0 and E14 detected 3, 88 and 197 differentially used exons, respectively (padj < 0.05, Supplementary Data 2). Interestingly, several marker genes of mDA neurons showed significant DEU, such as *Th* and *Aldh1a1* (Supplementary Fig. 3c, d). Other examples of genes with significant DEU were highly expressed lncRNAs, including *Malat1* and *Tia1*, or circRNA host-genes, such as *Tulp4* (Supplementary Data 2). AS events were determined by a more in-depth analysis (rMATS) and 1970, 1022 and 1698 significant events were found, respectively, for comparisons of E14 and P0, E14 and E16, and E16 and P0 (FDR < 0.05, ΔPSI > 0.1; Supplementary Fig. 3e, f, Supplementary Data 2). The majority of differential AS events were SE (Supplementary Fig. 3f). These results confirm that transcripts can undergo multiple types of AS events, as exemplified by the lncRNA *Rmst*, which has been linked to mDA neuron development (Supplementary Fig. 3g, h).

Next, circRNA prediction was performed using the timeseries data and identified 7529 circRNAs using CIRI2[47], of which 2966 were also detected by CIRCexplorer2[48] (Supplementary Data 2). The majority of timeseries RNAseq predicted circRNAs were generated from protein-coding host-genes (Supplementary Fig. 3i). CircRNAs in the timeseries dataset were predicted to consist of 5.1 exons on average, and chromosome 2 was a preferred site for circRNA production (Fig. 3b). Although PCA revealed clear sample separation based on circRNA expression, only two circRNAs were significantly differentially expressed between P0 and E16, and 38 between E14 to P0 (padj < 0.05, l2fc > 0.5 and l2fc < −0.5; Supplementary Data 2). The vast majority of transcripts in the dataset were linear, but a few genes predominantly produced circRNAs, as calculated by BSJ-to-exon ratios (Supplementary Fig. 4a–d, Supplementary Data 2). The most highly expressed circRNAs clustered at specific developmental stages, but only modest changes in circular-to-linear ratio were observed in time (Fig. 3c). Finally, to confirm the circRNA detection methods, the existence of predicted circRNAs that were experimentally assessed in this study was validated by RT-qPCR amplification of the BSJ in an independent bulk vMB sample (Fig. 3d).

Together, these results show expression of circRNAs during mDA neuron development, several of which display specific expression changes at critical developmental stages.

Subcellular localisation and knockdown of circRNAs in developing mDA neurons

While a few circRNAs have been studied in relation to mDA neuron differentiation in vitro or mDA neuron diseases (e.g[23,49].), the physiological role of circRNAs in mDA system development remains unknown. Therefore, to begin to define a potential role of circRNAs in developing mDA neurons, single-molecule fluorescence in situ hybridisation (smFISH) was performed in E14 vMB primary cultures. A few circRNAs were selected based on expression level and cell-type specificity (Fig. 4a, Supplementary Fig. 4e) and subsequent quantification was performed for three circRNAs to confirm these qualitative observations. CircRNAs (circ*Fat3*, circ*Lmx1a* and circ*Rmst*) were detected as early as 1 day in vitro (DIV1) in TH^+ mDA neurons and were still present at DIV5 (Fig. 4a–d). No significant enrichment of circRNAs in soma or neurites was found at DIV5, indicating that the selected circRNAs were expressed throughout the neuron (Fig. 4e).

Because the smFISH data identified circRNAs in different subcellular compartments in mDA neurons in vitro, we next performed circRNA knockdown (KD) in mDA neuron cultures to begin to understand potential roles of circRNAs in developing mDA neurons. To select circRNA candidates for KD experiments, E14 RNAseq data (Fig. 2) were analysed for significantly different and abundantly expressed circRNAs using specific parameters (padj < 0.05, l2fc > 0.5, baseMean > 40; Supplementary Data 1) (Fig. 4f). The selection using these parameters, which in our experience allow reliable subsequent visualisation and manipulation of circRNAs in neurons, yielded three candidates: circ*Lmx1a*, circ*Rmst* and circ*Fat3*. Next, the temporal expression profile of these candidates was assessed using the timeseries RNAseq data (Fig. 3). Expression levels of *circRmst* decreased in time (E14 to P0), whereas abundance of the other two candidates,

https://doi.org/10.1038/s41467-024-51041-1

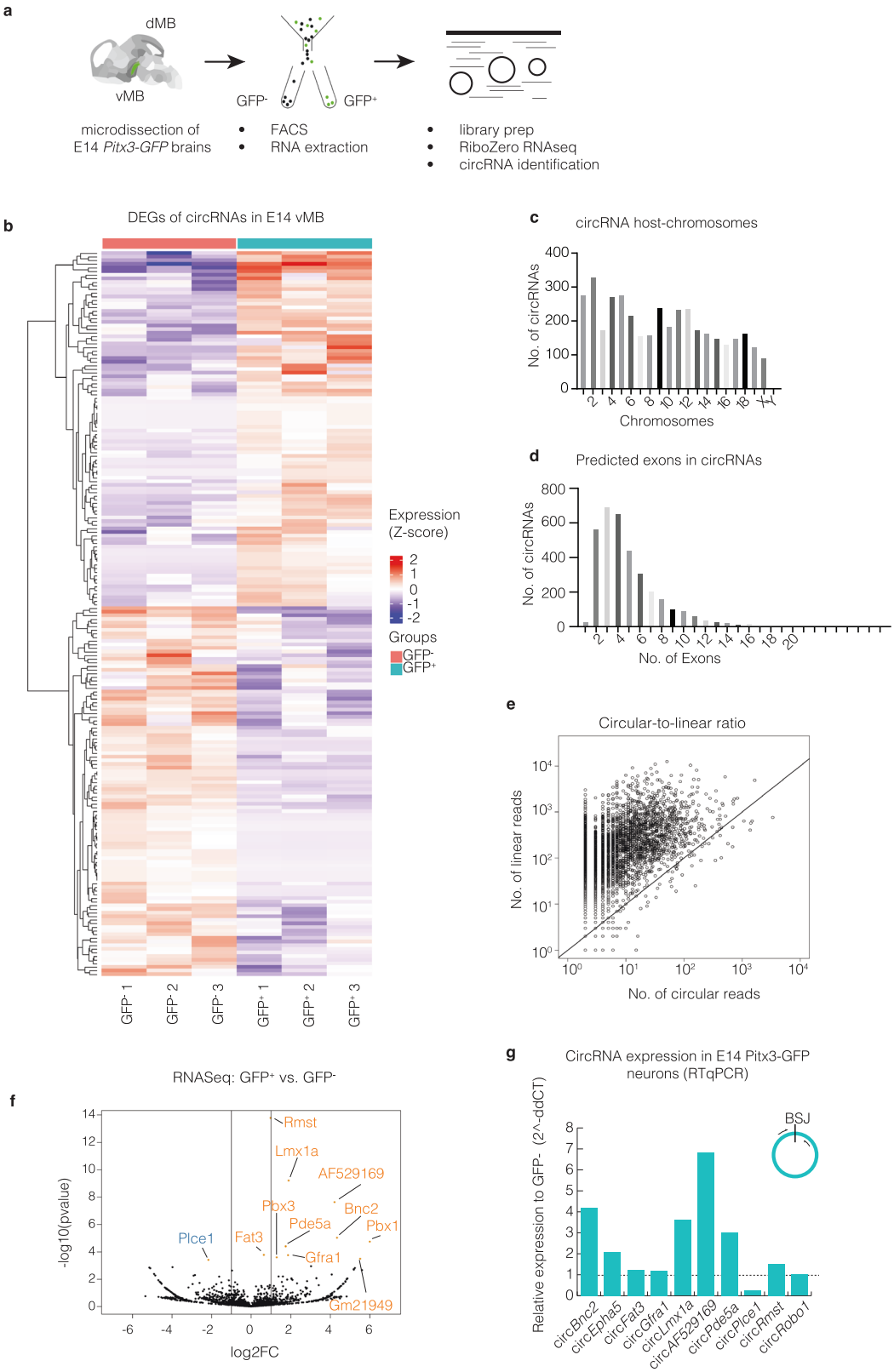

circFat3 and *circLmx1a*, was similar at the different timepoints (padj < 0.05, Supplementary Data 2). As controls for these differentially regulated circRNAs (downregulated or stable) in subsequent KD studies, we selected (1) *circTulp4*, as the most highly abundant circRNA (highest baseMean) in the timeseries RNAseq data that did not show expression changes in time (padj < 0.05, Supplementary Data 2), and (2) *circEzh2*, the most highly abundant circRNA in the timeseries RNAseq data that was downregulated in time (padj < 0.05, Supplementary Data 2). Interestingly, for the circRNA host genes *Ezh2*, *Lmx1a* and *Rmst* functional roles in mDA neurons had been established previously[50,51]. Three BSJ-spanning short-hairpin RNAs (shRNAs) were designed for each candidate in a lentiviral backbone (Fig. 4g). E14 primary vMB cultures were infected with shRNA-carrying lentivirus and harvested at DIV3 (Fig. 4h). For circ*Fat3* we had previously

Fig. 2 | Expression of circRNAs in embryonic mDA neuron development. **a** Schematic representation of the RNAseq method. E14 *Pitx3*$^{GFP/+}$ vMBs were dissociated and subjected to FACS. Purified mDA neurons (GFP$^+$) and non-mDA neurons (GFP$^-$) were subjected to rRNA depleted (riboZero) RNAseq and circRNA analysis. **b** Heatmap of top 200 differentially expressed circRNAs (DEseq2) from GFP$^+$ (mDA neurons) and GFP$^-$ samples (n = 3 each) from E14 *Pitx3*$^{GFP/+}$ vMB. CircRNA abundance is shown (as z-score) as ordered by differential expression between groups, no statistical cut-off was applied. Characterisation of detected circRNAs according to (**c**) chromosomal location, (**d**) predicted exon number per circRNA and (**e**) circular-to-linear ratio (depicted as BSJ containing reads (circular) plotted against linear reads of the E14 dataset). **f** Volcano plot showing all predicted circRNAs in the E14 RNAseq dataset. l2fc = 1 is indicated by vertical lines for visualisation. Significantly downregulated and upregulated circRNAs (padj < 0.05, l2fc > 0.5) are depicted in blue and orange, respectively and labelled by host gene name (*Plce1*, *Fat3*, *Rmst*, *Lmx1a*, *Pbx3*, *Pde5a*, *Gfra1*, *AF529169*, *Bnc2*, *Pbx1*, *Gm21949*). **g** Validation of the existence of predicted circRNAs from the E14 RNAseq data and their abundance in mDA neurons using an independent, purified E14 *Pitx3-GFP* sample (FACSed neurons) by RT-qPCR. Divergent, BSJ-spanning primers were designed to specifically amplify the BSJ. DE from RNAseq was confirmed for all predicted candidates. Upregulated in mDA neurons: circ*Bnc2*, circ*Epha5*, circ*Fat3*, circ*Gfra1*, circ*Lmx1a*, circ*AF529169*, circ*Pde5a*, circ*Rmst*, circ*Robo1*. Downregulated: circ*Plce1*. n = 1 (pooled FACS-sorted *Pitx3*$^{GFP/+}$ vMBs of 1 litter). No statistical test was performed. DEG differentially expressed genes, PCA Principal component analysis, log2FC log two-fold change. Source data are provided as a Source Data file and Supplementary Data file.

developed a KD approach[37] and levels of circ*Ezh2*, circ*Rmst* and circ*Tulp4* were shown here to be successfully reduced by one or more shRNAs. No specific KD could be obtained for circ*Lmx1a*. Therefore, KD experiments were performed for circ*Ezh2*, circ*Fat3*, circ*Rmst* and circ*Tulp4*.

Analysis of mDA neuron morphology following KD of circ*Ezh2*, circ*Fat3*, circ*Rmst* or circ*Tulp4* in E14 cultures (Fig. 5a, Supplementary Fig. 5a) did not show changes in the number of neurites, total branches or primary branches (Supplementary Fig. 5b–d). Similarly, overall neuron complexity, as assessed by Sholl analysis, was not significantly altered (Supplementary Fig. 5e). However, KD of circ*Tulp4* caused a small decrease in average neurite length and an increase in secondary branch count by 93% ($p < 0.05$; Fig. 5b–d). Quantification of circ*Rmst* KD cultures revealed a significant increase in soma size of 52% ($p < 0.001$; Fig. 5d–h). Increased soma size was also found for circ*Fat3* KD (23% increase, $p < 0.001$), but not following KD of circ*Ezh2* or circ*Tulp4* KD. To determine whether both cytoplasmic and nuclear compartments were enlarged following circRNA KD, nuclear area was quantified. Soma-to-nuclear-ratio was increased by 50% in circ*Rmst* KD cultures, confirming a cytoplasm-specific effect. Circ*Fat3* KD induced an enlargement of the soma and the nucleus, indicating enlargement of the entire neuron (Fig. 5f). Finally, at DIV3 a 19% decrease in the number of TH$^+$ neurons was found ($p < 0.00001$) in circ*Rmst* KD cultures but not following KD of the other candidates (Fig. 5i). Together, these data suggest that circRNA KD induces circRNA-specific changes in mDA neuron morphology and (TH$^+$) number.

Long-read sequencing reveals the composition of circ*Rmst* and other circRNAs

Our in vitro analysis of the effect of KD of different circRNAs showed that circ*Rmst* KD had the most wide-spread effects (e.g. a cytoplasm-specific effect on soma size, and TH$^+$ neuron number). Therefore, more in-depth analysis of this circRNA was performed. First, the composition of circ*Rmst* in mDA neurons was analysed. Our analysis of total RNA revealed a high number of alternative transcripts in mDA neurons (Supplementary Figs. 2e–h, 3c–h). CircRNAs are predicted based on their BSJ sequence as detected by RNAseq or RT-qPCR (e.g. Supplementary Fig. 6a, 6b) and most of their sequence is identical to linear transcripts from the same locus. This precludes identification of full circRNA sequences from regular short-read RNAseq data. Therefore, we next subjected purified mDA neurons to targeted long-read sequencing (LRS) using Oxford Nanopore Technology (ONT) to determine circRNA composition beyond the BSJ (Fig. 6a). In addition to circ*Rmst*, other circRNAs were included to provide a broader picture of circRNA diversity in developing mDA neurons. Primers were designed to target a preselected panel of circRNAs including mDA neuron-relevant circRNAs (e.g. circ*Rmst*, circ*Pbx1* and circ*Lmx1a*) or circRNAs with high expression in neural tissue (e.g. circ*Tulp4*, circ*Rims2* and circ*Fat3*) (circPanel-LRS[52]) (Fig. 6, Supplementary Fig. 6, Supplementary Data 3). The circPanel-LRS detected 97 circRNA isoforms with 100 or more BSJ-spanning reads (Supplementary Data 3) and revealed several novel and unique cryptic and circRNA-specific exons (Supplementary Fig. 6c–g). For optimal comparison of exon and intron structures, read counts were normalised and data were combined per time point (E14 or P0). Most cryptic novel (previously unannotated) circRNA-specific exons were larger than 29 bp, peaking around 41–60 bp (Fig. 6b–e). Unique novel exons distributed bimodally with a highest count of 3 bp (Fig. 6b, c, f–g). To understand alternative exon composition, the frequency of spliced exons was analysed. This revealed that short exons of 3–9 bp length are most frequently included, while exons of 17–23 bp were absent in P0 samples (Fig. 6h, i). Retained introns of circRNAs were up to 400 bp in length (Fig. 6j, k). More detailed analysis was performed for circ*Rmst*. By targeting a conserved locus, exon 4 (Refseq), 25 different isoforms of circular *Rmst* were found (with different BSJs), of which eight isoforms had not been annotated previously (Supplementary Data 3). Furthermore, a novel exon, included in both *Rmst* and circular *Rmst*, was discovered downstream of Refseq exon 13 (Supplementary Fig. 6h). Retrieval of the consensus sequence of the circ*Rmst* candidate selected in this study, *mmu_circ_0000205*, revealed two isoforms with the same BSJ. These differed by the inclusion of exon 11 (Refseq). The spliced-in rates of exon 11 were 30% and 60% at E14 and P0, respectively (Supplementary Data 3). This suggests that circ*Rmst* exon 11 may play a critical role as development progresses.

Together, these data begin to provide insight into the molecular composition of circRNAs in developing mDA neurons, including a more detailed understanding of circ*Rmst*. Further, these results highlight intriguing temporal changes that may affect circRNA structure and function.

circ*Rmst* displays VTA-enriched expression and its knockdown has developmental, stage-dependent effects

The abundance of neuronal phenotypes following circ*Rmst* KD and its interesting molecular composition (Supplementary Fig. 6h, Supplementary Data 3) prompted us to study this circRNA in more detail. Therefore, we first performed additional KD and expression analyses to confirm the specific effects of circ*Rmst* KD on mDA neuron morphology (Fig. 5) and to further unveil the consequences of reducing the levels of this circRNA.

First, to control for possible off-target effects of the KD approach, another KD method was developed, i.e. post-transcriptional RNA degradation using CasRx[53] (Fig. 7a–c). Several guide RNAs (gRNAs) targeting the BSJ (DRg) were designed of which one (DR g2) induced circ*Rmst* KD without changing linear *Rmst* expression (Supplementary Fig. 7c). CasRx-mediated KD of circ*Rmst* also induced changes in soma size and TH$^+$ neuron number in E14 vMb primary cultures, similar to shRNA-mediated KD (Fig. 7c, Supplementary Fig. 7a, b). In addition, CasRx-mediated knockdown of circ*Rmst* also reduced the TH$^+$ neuron number (Fig. 7c). Together, these data suggest that specific KD of the circular form of *Rmst* (in the absence of changes in the linear isoform) induces various phenotypes in mDA neurons (Figs. 5, 7). However, since the linear

https://doi.org/10.1038/s41467-024-51041-1

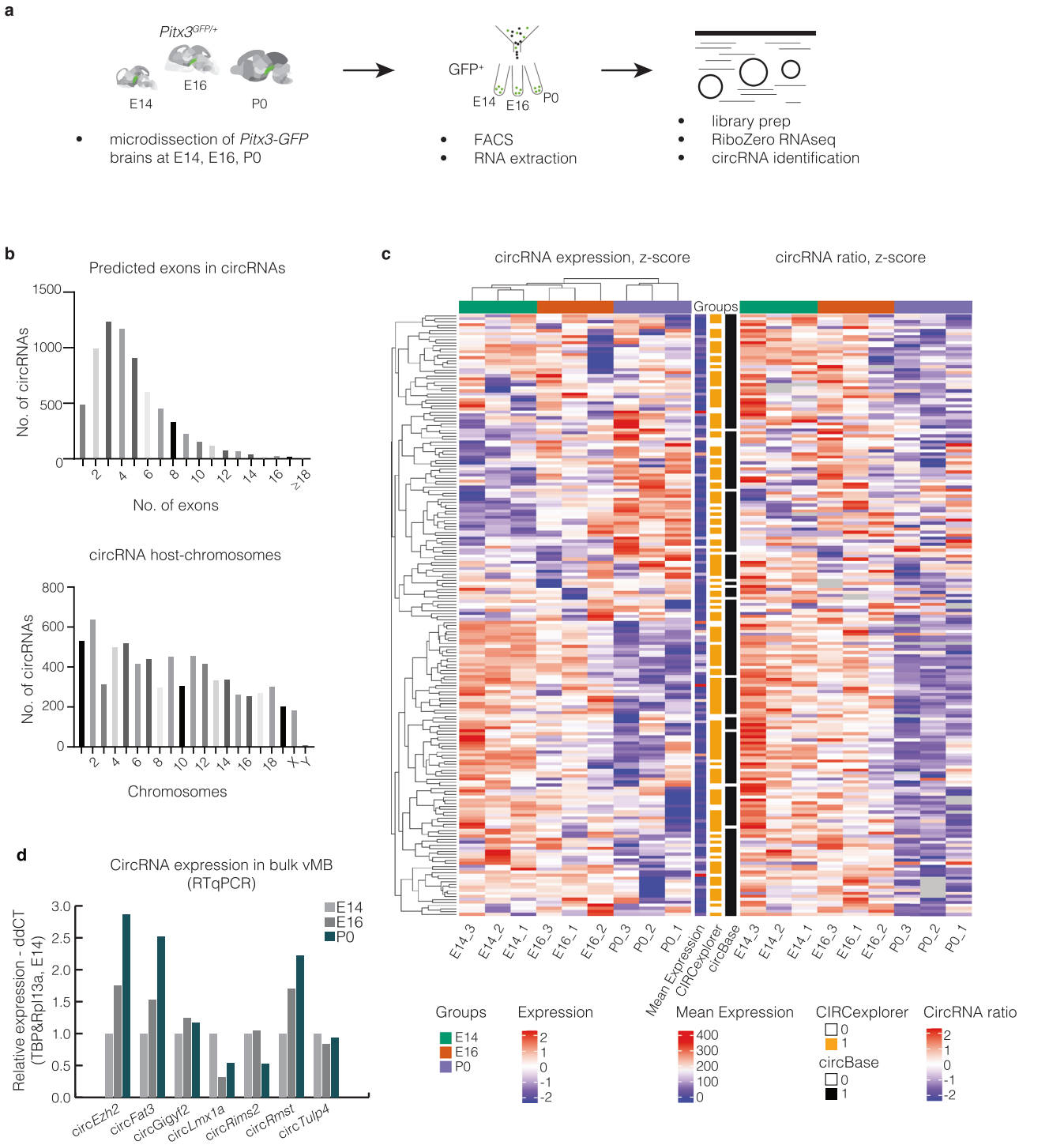

Fig. 3 | Temporal dynamics of circRNA expression in developing mDA neurons. **a** Schematic representation showing the collection of GFP⁺ mDA neurons. Dissection of E14, E16 and P0 *Pitx3*$^{GFP/+}$ vMBs was followed by FACS sorting, rRNA-depleted RNAseq and circRNA analysis. **b** Categorisation of detected E14, E16, P0 *Pitx3-GFP* neuron circRNAs according to predicted exon number per circRNA (upper panel) and chromosomal location (lower panel). **c** Differential expression (DESeq2) of circRNAs (left heatmap) and circular-to-linear ratio (right heatmap) between the E14, E16 and P0 stages (groups); between heatmaps mean expression, CIRCexplorer detection (binary) and circBase detection (binary) are plotted; colour codes in the legends. n = 3 samples per developmental stage. **d** Validation of select candidate circRNAs from RNAseq data (timeseries) by RT-qPCR. Candidates (circ*Ezh2*, circ*Fat3*, circ*Gigyf2*, circ*Lmx1a*, circ*Rims2*, circ*Rmst*, circ*Tulp4*) were confirmed by BSJ amplification from pooled bulk vMBs of E14, E16 and P0 WT brains. Housekeeping genes: *Tbp* and *Rpl13a*. n = 1, no statistical test was performed. Source data are provided as a Source Data file and Supplementary Data file.

lncRNA *Rmst* has also been associated with mDA neuron development[54], we also attempted to test the effect of specifically depleting linear *Rmst*. However, none of the shRNAs tested induced KD of linear *Rmst* in mDA neuron cultures without changing circ*Rmst* (e.g. Supplementary Fig. 7d).

KD of *circRmst* led to a consistent reduction in TH⁺ neuron number in vitro. Since different subtypes of mDA neurons have been described, it is possible that this reduction reflects changes in or loss of specific subtypes. To assess this hypothesis, we first examined whether circ*Rmst* is expressed in distinct parts of the developing mDA system

https://doi.org/10.1038/s41467-024-51041-1

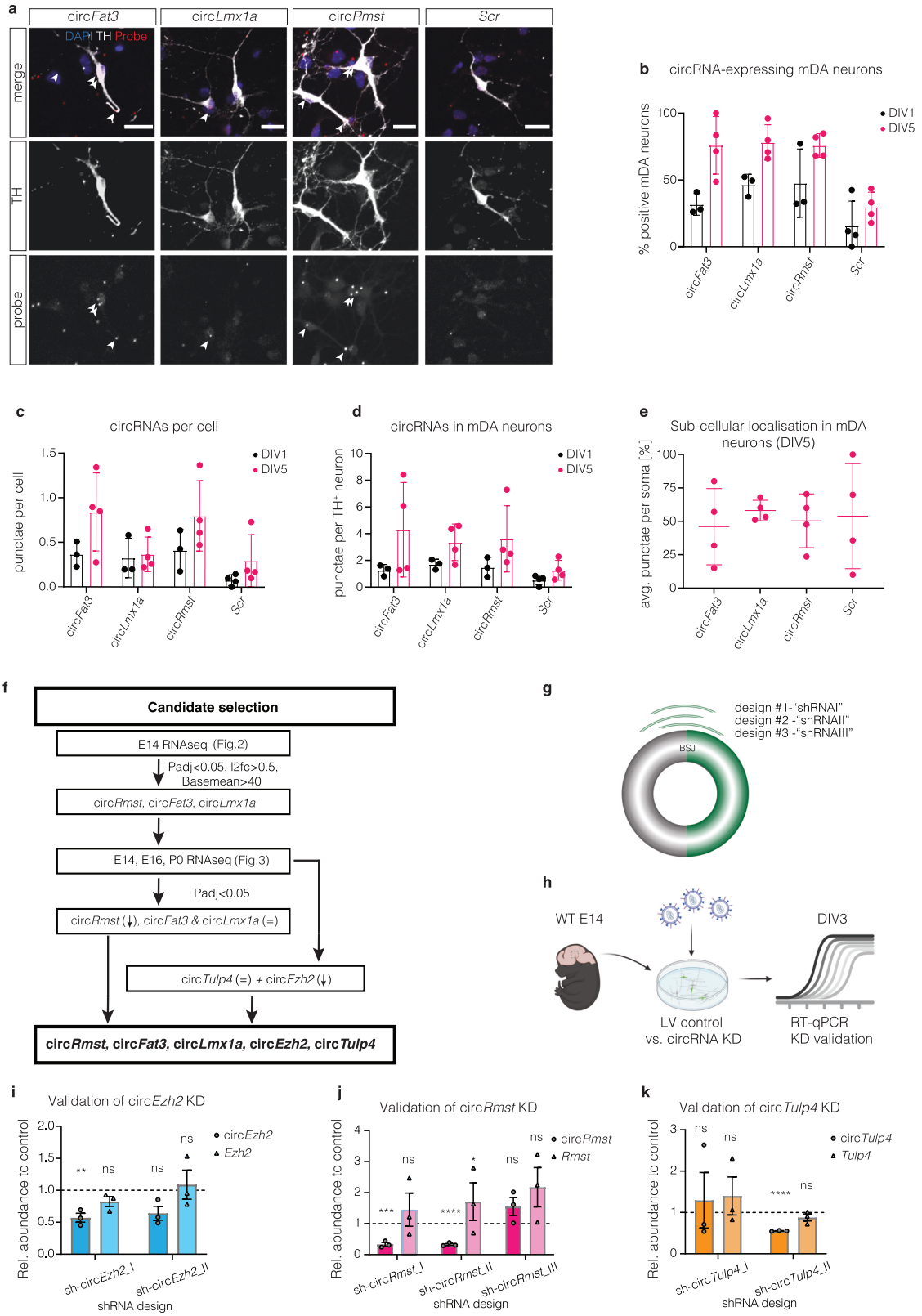

(VTA versus SNc) using two different methods. RT-qPCR of mDA neurons (Pitx3-GFP$^+$) purified from E16 VTA or SNc showed that both *Rmst* and circ*Rmst* are enriched in VTA as compared to SNc mDA neurons at E16 (Fig. 7d, e). Analysis of circ*Rmst* expression by LNA-based fluorescent in situ hybridisation (LNA-FISH) confirmed this interesting observation, showing strong overlap between circ*Rmst* signal and TH expression in the E14 VTA region (Fig. 7f). Based on these observations, circ*Rmst* KD was performed in mDA neuron cultures followed by immunocytochemistry for markers of VTA and SNc. The percentage of VTA (CALBINDIN1$^+$) and SNc (GIRK2$^+$) mDA neurons did not differ between circ*Rmst* KD and control cultures (Fig. 8a, b). Thus, while circ*Rmst* shows VTA-enriched expression, these data suggest that this circRNA does not regulate the development of specific mDA neuron subtypes.

Fig. 4 | Subcellular localisation and knockdown of circRNAs in vitro. a Single-molecule fluorescence in situ hybridisation (smFISH) of circ*Fat3*, circ*Lmx1a*, circ*Rmst* and a scrambled control (Scr) in E14 vMB primary cultures at DIV5. In merged image: DAPI = blue, TH = white, smFISH probe = red. White arrows indicate signal in mDA neurons. Scale bars = 20 μm. **b**–**e** Quantification of smFISH in vMB cultures as in a. **b** Probe signal in mDA neurons in vMB primary cultures at DIV1 versus DIV5. Data presented as percentage of positive mDA neurons (of all mDA neurons). **c** Quantification of detected signal (punctae) per cell (punctae per DAPI signal) at DIV1 versus DIV5. **d** Quantification of detected signal (punctae) per mDA neuron at DIV1 versus DIV5. **e** Quantification of subcellular localisation (soma vs. neurites) of circRNAs at DIV5. **b**–**d** n = 3 cultures (DIV1), n = 4 cultures (DIV5), (**e**) n = 3–4 cultures. Data are shown as means ± SD, (**b**–**d**) multiple unpaired two-sided t-tests with Holm Sidak multiple testing, (**e**) ordinary one way ANOVA with Tukey's multiple comparisons test, (**b**–**e**) all n.s. adjusted $P > 0.05$. **f** Schematic overview of the selection of circRNA candidates for KD experiments. **g** Schematic representation of shRNA design. Three shRNAs were designed for each BSJ. One directly on top of the BSJ (design #1, 'shRNAI'), 3 nts upstream (design #2, 'shRNAII') and 3 nts downstream (design #3, 'shRNAIII'). **h** Schematic representation of circRNA knockdown (KD) in primary cultures of dissociated E14 WT vMBs. Corresponding shRNAs were delivered via LV infection to control and KD cultures, respectively. At DIV3, circRNA KD cultures were subjected to RT-qPCR for KD validation. Figure contains icons from BioRender.com. circRNA KD validation as relative expression of circRNA or linear counterpart RNA to control cultures for (**i**) circ*Ezh2*, (**j**) circ*Rmst* and (**k**) circ*Tulp4*. For each circRNA candidate three shRNAs were designed. Results of all constructs with successful plasmid cloning are shown. Sh-circEzh_I, sh-circRmst_I and sh-circTulp_II were selected for further experiments. n = 3 primary cultures, multiple unpaired two-sided t-tests, with Holm-Sidak multiple testing, mean ± SEM, (**i**) $^{**}P = 0.007175$, (**j**) $^{***}P = 0.000694$, $^{****}P = 0.000053$, (**k**) $^{****}P = 0.000001$. Source data are provided as a Source Data file.

The number of ENGRAILED1$^+$ or NURR1$^+$ neurons was also unchanged following circ*Rmst* KD, arguing against a stage-specific role for circ*Rmst* in mDA neuron formation (Fig. 8a, b). However, as it is possible that circ*Rmst* serves other functions at early developmental stages, shRNA-mediated KD was performed in E11 vMB primary cultures followed by analysis at DIV3 (Supplementary Fig. 7e–g). No difference in the relative number of TH$^+$ neurons was observed, suggesting that circ*Rmst* may play a role in mDA neuron maintenance and survival, rather than cell type-specification (Supplementary Fig. 7f). However, consistent with our previous findings, a significant increase in soma size was found, in addition to small differences in initial neurite number and length (Supplementary Fig. 7f, g). Together, these results suggest developmental stage-specific roles for circ*Rmst* in the regulation of mDA connectivity, soma size and neuron number.

circ*Rmst* knockdown accelerates mDA neuron migration in vivo

Our data identify subregion-specific expression levels and different effects of circ*Rmst* KD in developing mDA neurons. These interesting features triggered us to examine a potential mechanism-of-action for circ*Rmst* in mDA neurons. First, the effect of circ*Rmst* KD on gene expression was investigated to identify pathways that may explain the observed in vitro phenotypes (Fig. 8c, d). RNA from DIV3 cultures was subjected to total RNAseq which resulted in the identification of 149 DEGs ($p < 0.05$) that contributed to pathways such as integrin signalling (*Arpc3*, *Col1a1*, *Col8a1*, *Fn1*), Parkinson disease (*Mcm3*, *Pbx3*, *Septin5*, *Sncb*) and DA transport (*Adcy2*, *Epb41*, *Gng4*; Supplementary Data 4). However, due to high variability and modest expression changes only one statistically significant DEG (padj < 0.05) was detected after adjusting for multiple testing, namely *Gm24019*, which is predicted to code for a U6 small nuclear RNA (snRNA)[55]. CircRNAs have been reported to bind and regulate RBPs and miRNAs. Therefore, to gain further insight into the potential pathways downstream of circ*Rmst*, in silico predictions for putative RBP and miRNA binding partners of circ*Rmst* were performed and assessed using pathway analysis (Supplementary Fig. 8, Supplementary Data 5). miRNA target mining predicted 3633 genes, which were classified into 136 pathways. Pathway analysis of miRNA target genes implicated circ*Rmst* in neuron development and hinted at roles in mDA neuron progenitor proliferation (WNT signalling[54,56]), mDA neuron morphology (Integrin signalling[57], PI3K pathway[58]) and neuron migration (Integrin signalling[59]) (Supplementary Data 5). Pathways shared between both miRNA/RBP prediction and RNAseq analysis high-lighted potential roles for circ*Rmst* in the regulation of cell morphology and migration (e.g. integrin signalling). Circ*Rmst* is expressed at the time of mDA neuron migration, and the in vitro phenotypes observed suggest that this circRNA regulates neuronal morphology, which is crucial for migrating neurons[9]. To investigate a potential role for circ*Rmst* in mDA neuron migration in vivo, *Pitx3*$^{cre/+}$ embryos were subjected to *in utero* electroporation (IUE) at E12 (Fig. 9a). Co-injection of a Cre-specific reporter, *iSureCre*[60] and a shRNA-expressing plasmid (*pll3.7-sh-circRmstI*) or scrambled control vector was performed. After electroporation of the vMB, embryos were collected at E18 and the position of RFP$^+$ mDA neurons along the dorsal-ventral (y)- and medial-lateral (x)-axes was determined. This revealed a more lateral position of circ*Rmst* KD mDA neurons as compared to control mDA neurons (Fig. 9b–d). The location of neurons along the y-axis did not differ significantly (Fig. 9c, d). These findings support a role for circ*Rmst* in mDA neuron migration and the lateral positioning of these neurons. Electroporated mDA neurons did not show overt morphological changes but incomplete filling of neurons with RFP precluded a more detailed analysis of neuronal morphology at E18.

To further define the effect of circ*Rmst* KD on mDA neuron migration, live-cell imaging of ex vivo electroporated organotypic slice cultures was performed (Fig. 10a). E12 *Pitx3*$^{cre/+}$ vMBs were electroporated with sh-circRmst I or a scrambled control. At DIV1, slices were imaged for several hours and electroporated mDA neurons were analysed for parameters describing the path and speed of neuron migration (Fig. 10a–d). To ensure specificity, co-electroporated *iSureCre*$^+$ mDA neurons were analysed. Track length was increased ($p < 0.001$) but migratory track straightness was unchanged, suggesting that migratory pathfinding was intact (Fig. 10b). However, cell tracking revealed a significant increase in mean ($p < 0.005$) and maximum speed ($p < 0.001$) and speed variation ($p < 0.01$) in KD neurons (Fig. 10c). This supports our in vivo findings showing a more lateral position of KD neurons further from the ventricle (Fig. 9). Thus, we propose that circ*Rmst* contributes to the regulation of mDA neuron migration by controlling migration speed.

Discussion

The development of mDA neurons is governed by a myriad of molecular factors. However, despite abundant neuronal expression and established functions in neural development, the role of long ncRNAs in developing mDA neurons has remained largely unexplored. Here, we established a comprehensive map of the genome-wide expression profiles and splicing patterns of a specific and poorly defined class of long ncRNAs, circRNAs, at key developmental stages in mouse mDA neurons. This analysis revealed insights into the dynamic expression levels and regulation of circRNAs in mDA neurons in vivo (Fig. 10e). Subsequent functional analyses suggest unreported and specific physiological roles for a select group of circRNAs (circ*Ezh2*, circ*Fat3*, circ*Rmst* and circ*Tulp4)* and more detailed studies indicate a contribution of circ*Rmst* to the regulation of mDA neuron morphology and soma size in vitro, and neuron migration in vivo. These results, for the first time, implicate circRNAs in mDA neuron development, add another layer of complexity to the molecular regulation of mDA neuron migration and provide a resource for further dissection of the role of circRNAs during mDA development.

https://doi.org/10.1038/s41467-024-51041-1

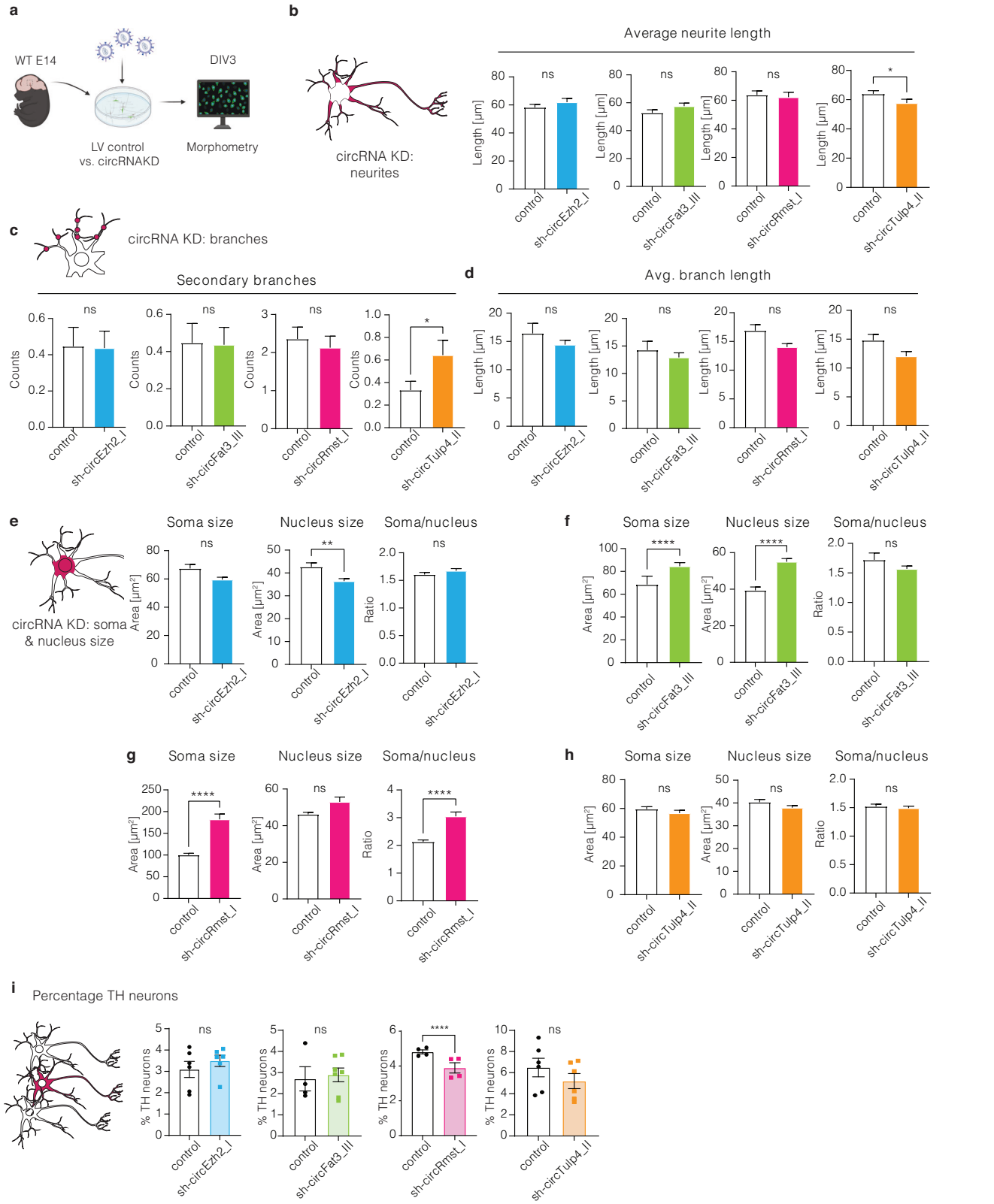

Circular RNA expression and splicing during mDA development

Our results establish the abundance, cell type-specificity and expression patterns of circRNAs during mDA neuron development. They define circRNA expression patterns in developing mDA neurons, but also uncover previously unidentified structural elements (e.g. exon 14 in the *Rmst* locus). Further, our data highlight a high degree of temporal regulation of the expression and composition of circRNAs in developing mDA neurons. These include, for example, inclusion of micro-exons, increased inclusion of specific exons during development (exon 11 in circ*Rmst*) and differences in AS events between developmental timepoints. The functional consequences of these and other temporal changes remain to be explored.

A few previous studies have examined the expression and in vitro effects of lncRNAs in human and mouse mDA neurons[16,61], but the

Fig. 5 | Analysis of mDA neuron morphology and number after circRNA knockdown. a Schematic representation of the experimental approach. circRNA knockdown (KD) was performed on E14 WT vMB primary cultures and induced by lentiviral (LV)-mediated delivery of shRNAs. At DIV3, circRNA KD cultures were immunostained for TH and subjected to morphometry. Figure contains icons from BioRender.com. **b**–**i** Morphometry of TH$^+$ neurons transduced with shRNA (targeting circ*Ezh2*, circ*Fat3*, circ*Rmst*, or circ*Tulp4*) versus control. Schematics visualise the morphological features that are quantified. Quantification of (**b**) average neurite length, (**c**) number of secondary branches, and (**d**) average branch length show significant changes upon KD of circ*Rmst*. **e**–**h** Analysis of soma size, nucleus size and soma-to-nucleus size-ratio reveal significant changes in circ*Ezh2*, circ*Fat3* and circ*Rmst* KD cultures. **b**–**d**, **e** n = 65 (GFP) & 71 (shcircEzh_I) neurons, (**b**–**d**, **f**) n = 55 (GFP) & 89 (shcircFat3_III) neurons, (**b**–**d**, **g**) n = 130 (GFP) & 127 (shcircRmst_I) neurons, (**b**–**d**, **h**) n = 84 (GFP) & 70 (shcircTulp4_II) neurons, (**g**) n = 127 (GFP) & 130 (shcircRmst_I) neurons, **b**–**i** normality tested with Shapiro-Wilk, two-sided t-test or two-tailed Mann Whitney U tests, mean ± SEM, (**b**) $^*P = 0.0171$, (**c**) $^*P = 0.0219$, (**d**) $^*P = 0.0134$, (**e**) $^{**}P = 0.0089$, (**f**) $^{****}P = 0.0001$ (both), (**g**) $^{****}P = 0.0001$ (both). **i** Quantification of the percentage of TH$^+$ neurons in the different cultures. circ*Rmst* KD induces a reduction in the number of TH$^+$ neurons. n = 4 cultures, two-sided t-tests or two-sided Mann Whitney U tests, mean ± SEM, $^{*****}P < 0.00001$. KD knockdown, LV lentivirus, TH tyrosine hydroxylase, vMB ventral midbrain, WT wildtype. Source data are provided as Source Data file and Supplementary Data files.

functional role of circRNAs remained unaddressed. Our short-read RNAseq analysis and circRNA LRS identified many differentially spliced circRNAs in mDA neurons exhibiting many unannotated circRNA-specific exons and AS events. Further, analysis of a select number of circRNAs, i.e. mDA neuron-relevant or highly expressed circRNAs, identified alternative exon usage for specific circRNAs. Although this approach did not allow comparison with non-mDA cells, it revealed that within mDA neurons alternative circRNA isoforms with a common BSJ exist. Unexpectedly, comparison of the circRNA transcriptome of E14 mDA neurons to that of other cells in the mDA area only identified a limited set of mDA-neuron enriched circRNAs. This is in sharp contrast to mRNA profiles, which differed markedly between mDA neurons and surrounding cells. A possible explanation for this difference is that many circRNAs are lowly expressed which may have precluded detection of their differential expression. Current methods for circRNA detection rely on computational prediction algorithms. This approach is, even if multiple lines of evidence are combined, associated with limitations[20,62]. Therefore, it is crucial to validate circRNAs with independent methods and experimentally assess their cellular and molecular functions.

Analysis of the localisation of a few selected circRNAs by smFISH confirmed their expression in mDA neurons in vitro. These circRNAs were detected at early stages, displayed increased expression as cultures matured and showed different levels in individual mDA neurons. Such heterogeneous expression may reflect mDA neuron subtype-specific circRNA expression. For example, circ*Rmst* is enriched in the VTA as compared to SNc region in vivo, which may explain differences in circ*Rmst* expression in cultures that contain neurons from both regions. Although previous work showed enrichment of circRNAs at synapses[33,34] no specific subcellular distribution of circRNAs was found in developing neurons in vitro. Nevertheless, circRNA signals were observed in both soma and neurites suggesting that circRNAs may function in both subcellular compartments.

Circ*Rmst* regulates the number of TH$^+$ neurons

Knockdown of distinct circRNAs caused changes in neuronal morphology and TH$^+$ neuron number in vitro, most likely reflecting different functions and downstream pathways. Circ*Rmst* KD had the most wide-spread effects (e.g. soma size and TH$^+$ neuron number) and therefore circ*Rmst* was selected to study the functional role of circRNAs in developing mDA neurons in more detail. This circRNA was strongly expressed in mDA neurons, both in vitro and in vivo, displayed subregion-specific expression and showed temporal changes in its molecular composition during development. Knockdown of circ*Rmst* in E14 vMB cultures using different experimental approaches consistently induced an increase in mDA soma size and a decrease in the number of TH$^+$ mDA neurons. Interestingly, these effects were in part developmental stage-dependent. Knockdown in younger cultures (E11) resulted in increased soma size, but not in changes in the number of TH$^+$ neurons. Further, KD at E11 induced fewer neurites with increased average length, while KD at E14 neurites were unchanged. There are several possible explanations for these differences. First, the observed phenotypes may simply reflect the stage at which specific cellular events occur (e.g. neurite growth precedes branching[63]). Second, circ*Rmst* (isoforms) and/or its interaction partners may display specific spatiotemporal expression and therefore circ*Rmst* manipulation could have specific temporal effects. For example, circ*Rmst* is enriched in the VTA and the generation of SNc mDA neurons precedes that of mDA VTA neurons[64,65]. It is important to note that circ*Rmst* KD was performed in vMB primary cultures, which are enriched for mDA neurons, but also contain other cell types. Despite high circ*Rmst* levels in mDA neurons, it is formally possible that circ*Rmst* KD in non-mDA cells contributed to the observed phenotypes. In future experiments, such contribution could be studied by performing mDA neuron-specific KD, as performed for the electroporation studies.

Whether circ*Rmst* regulates the number of mDA neurons and/or TH expression remains unknown but no differences in mDA neuron subsets or developmental markers were found. Previous studies have revealed an association between the mDA progenitor pool, midbrain size and WNT signalling[54,66–68]. LMX1b drives WNT1/WNT signalling and promotes the expression of (lncRNA) *Rmst*. *miR-135a*, also expressed from the *Rmst* locus, represses LMX1b and WNT targets[54]. Together, LMX1b and *miR-135a* have been proposed to modulate WNT signalling, thereby regulating the mDA neuron progenitor pool[69]. circ*Rmst* may also act via the *miR-135a*/LMX1b/WNT axis as KD of this circRNA affects *miR-135a* expression in the absence of changes in *Rmst* (Supplementary Fig. 9). However, circ*Rmst* lacks the *miR-135a* binding site present in the lncRNA *Rmst* and thus regulates this miRNA via distinct mechanisms.

Co-regulation of soma size and neuron migration by circ*Rmst*

The mechanisms that control neuronal soma size are incompletely understood. Increased soma size can be caused by different changes, including cytoskeletal, metabolic or electrophysiological alterations[70–73]. Based on circ*Rmst* pathway analysis (in silico and RNAseq) and mDA neuron morphology changes in vitro (e.g. elongated edges reminiscent of enlarged lamellipodia or changes in neurite formation and branching), it is tempting to speculate that cytoskeletal changes underlie the observed increase in soma size. At the molecular level two interacting signalling pathways have been studied most intensely in the context of soma size control: mammalian target of rapamycin (mTOR) and phosphatidyl-inositol-3-kinase (PI3K) signalling[71,74]. Tumour suppressor phosphatase and tensin homologue (PTEN) counteracts PI3K and is a negative regulator of mTOR thereby connecting these pathways. During embryonic development, mTOR regulates progenitor cell proliferation, differentiation and neuronal migration[75–77]. Deletion of *Pten* or *tuberous sclerosis complex 1* (*Tsc1*), both negative regulators of mTOR, leads to increased soma size and elevated DA synthesis[58,71,78]. Interestingly, analysis of the miRNA binding partners of circ*Rmst* identifies PI3K signalling as a significantly overrepresented pathway. Further, several predicted binding partners of circ*Rmst* (*mmu-miR-152-3p*, *mmu-miR-148a-3p* and *mmu-miR-148b-3p*) target PTEN (Supplementary Data S5).

https://doi.org/10.1038/s41467-024-51041-1

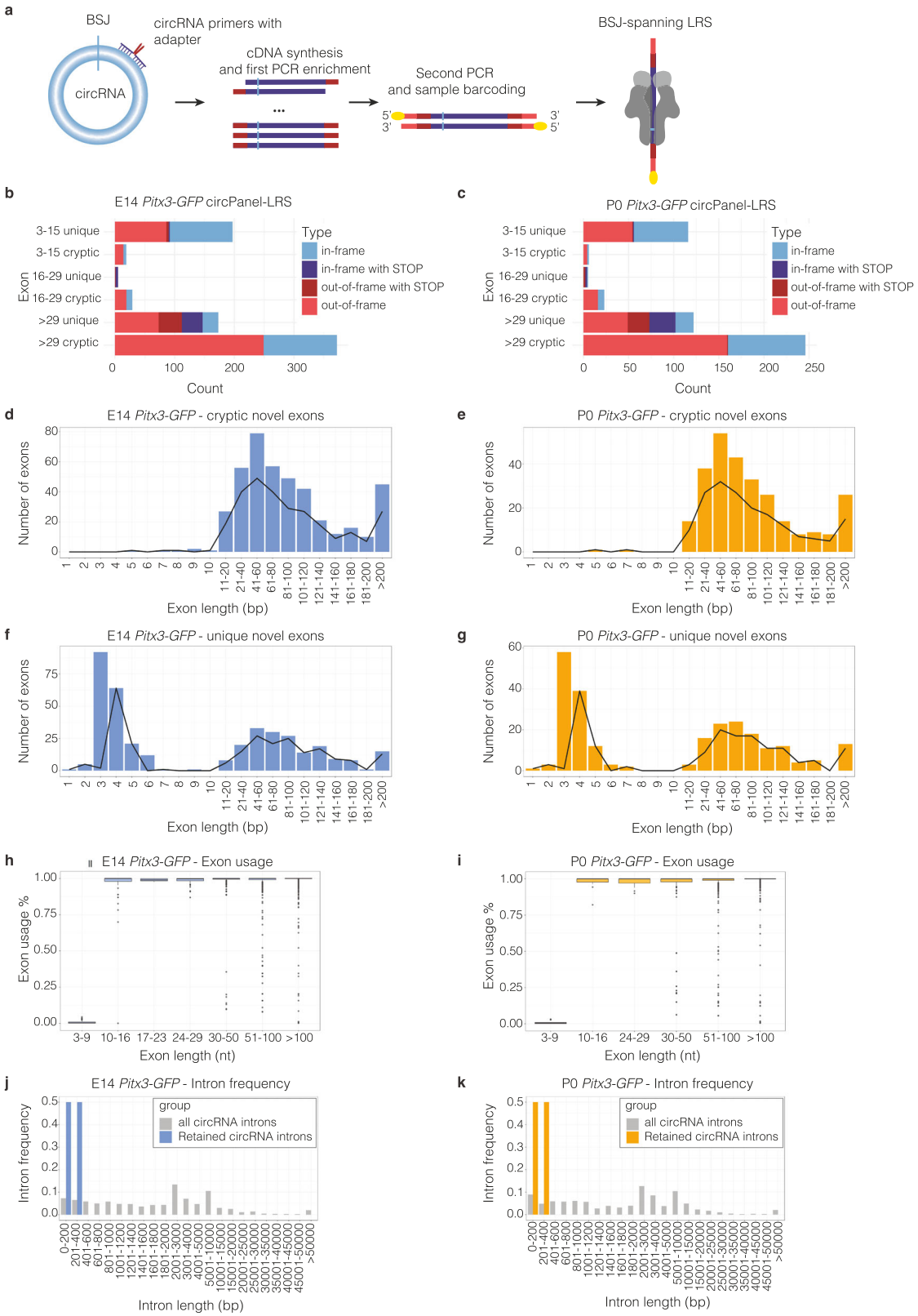

While future studies are needed to explore a potential link between circ*Rmst* and mTOR/PTEN signalling, it is interesting to note that PTEN not only regulates neuronal soma size[58,71], but also neural migration[79]. In addition to soma size changes, knockdown of circ*Rmst* in mDA neurons caused an increase in neuron migration in vivo (exemplified by a more lateral position of electroporated neurons). This was mirrored by an increase in migration speed following circ*Rmst* KD in organotypic slices. Early developmental processes such as cell fate specification and differentiation in the mDA system have been studied extensively, but cellular events that occur at later developmental stages, such as regulation of neuronal morphology or migration are less well understood[1,3–5]. Our data showing that circ*Rmst* impacts neurite number, length, soma size and neuron migration help to fill this void and add a new type of

Fig. 6 | Long-read sequencing of developing mDA neurons to investigate the molecular composition of circRNAs. a–k Normalised Oxford Nanopore Technology (ONT) sequencing data of circRNAs from FACS-sorted E14 and P0 *Pitx3-GFP* mDA neurons (n = 3 samples per developmental stage). **a** Simplified schematic of circRNA ONT sequencing (circPanel-LRS). Extended circRNA-specific divergent primers are designed downstream of the BSJ. After cDNA synthesis, samples are subjected to amplification using barcoded primers followed by the ligation of the sequencing adaptor and the multiplex final library subjected to ONT sequencing. Stacked barplots showing exon counts of (**b**) E14 and (**c**) P0 *Pitx3-GFP* neuron circPanel-LRS. Exons are categorised according to size (bp) and type (unique, cryptic). **d–k** Characterisation of ONT sequencing data from E14 and P0 *Pitx3-GFP* neurons. **d**, **e** Number of cryptic novel exons as shown by exon length. **f**, **g** Number of unique novel exons as shown by exon length. **h**, **i** Exon usage percent categorised by length. The box covers the Interquartile range (IQR), including the first to the third quartile (Q1 to Q3) with a horizontal black line representing the median. Whiskers, extending from both ends of the box, indicate the variability outside Q1 and Q3. Minimum whisker values are Q1 − 1.5 * IQR. Maximum whisker values are Q3 + 1.5 * IQR. Dots outside the whiskers are outliers. For each group (P0 and E14) ONT RNAseq reads for individual triplicates were concatenated, filtered and capped at 2.4 mio filtered reads, prior to ONT circRNA analysis. Plots in Fig. 6 show results from the concatenated datasets. Plots are made using ggplot. **j**, **k** Intron frequency as shown by intron length. circPanel-LRS circRNA panel long-read sequencing, BSJ backsplice junction, Pitx3 Pituitary homeobox 3. Source data are provided as a Supplementary Data file.

regulator, circRNA, to the control of mDA neuron development. mDA neuron migration is a three-dimensional process, as these neurons extend along the dorso-ventral, medio-lateral and caudo-rostral axes[8,10], that remains poorly characterised. Initial radial mDA neuron migration is mediated by extrinsic cues such as CXC-motif receptor 4 (CXCR4)/CXCL12 and deleted in colorectal cancer (DCC)/NETRIN-1[7,8,10]. In the vMB, SNc neurons change direction and continue to migrate tangentially (laterally), which is mediated by binding of RELN to the transmembrane receptors ApoE Receptor 2 (APOER2) and Very Low-Density Lipoprotein Receptor (VLDLR)[8,9,80–82]. Once in the SNc, axon-derived NETRIN-1 functions to attract GABAergic neurons into the SN pars reticulata thereby restricting mDA neurons to the SNc[10]. Interestingly, RELN signalling promotes laterally biased movements of migrating mDA SN neurons by increasing the probability of fast, laterally directed migration[9]. Thus, while several cell-extrinsic regulators of mDA neuron migration have been reported, the cell-intrinsic cues involved were unknown. The timing of the electroporation experiments in our study were aimed at targeting VTA mDA neurons as circ*Rmst* was predominantly expressed in the VTA. It is possible that a subset of SN mDA was also targeted by this approach and that in these cells circ*Rmst* affects the RELN pathway to modulate mDA neuron migration. However, as RELN has been found to primarily affect SN mDA neurons, circ*Rmst* is likely to function via other mechanisms in VTA mDA neurons. For example, circ*Rmst* may target PTEN through miRNA-dependent mechanisms or act via other binding partners such as RBPs. Several of the RBPs predicted to bind circ*Rmst* have been linked to cell migration or cytoskeletal dynamics (TAF15, U2AF2, RBFOX2, TARDBP, CELF1, HuR[83–92]). Although further studies are needed to dissect the mechanisms through which circ*Rmst* influences mDA neuron migration these data implicate a novel type of cell-intrinsic regulator in the control of mDA neuron migration.

In summary, our data provide a unique overview of the cell type-specific and developmentally dynamic regulation of circRNAs during mouse mDA neuron development that can be exploited in the future to establish the role of an exquisitely large group of these poorly characterised molecular factors in these neurons. In addition, our results implicate circRNAs in the migration of a mDA neuron subtype in vivo and expand our rather rudimentary understanding of the intrinsic molecular control of processes such as mDA soma size regulation and neuron migration. Together, our data provide a resource for dissecting how circRNAs regulate developmental programmes in mDA neurons and a starting point for future interrogation of circRNAs in disease states and therapeutic strategies.

Methods

A complete version of the Methods including detailed buffer composition, primer sequences and probe sequences is available in the Supplementary Information.

Animals

All animals were taken care of and used as model systems according to institutional guidelines, the Dutch law (Wet op Dierproeven 1996), European regulations (Guideline 86/609/EEC), in agreement with the Animal welfare body (IvD Utrecht) and approved by the (CCD) Centrale Commissie Dierproeven of Utrecht University (CCD license: AVD115002016532). Mice were housed socially and kept under a 12:12 h light-dark cycle with lights off at 19:00. All animals were kept at room temperature (21 ± 2 °C) and 40–70% humidity conditions. Food and water were supplied ad libitum. Counting of gestational age started with embryonic day 0 (E0) on the day at which the vaginal plug was detected. Male and female mice were used for the experiments. *C57BL/6* mice are referred to as wildtype (WT) and were obtained from Charles River Laboratories. *Pitx3-GFP* mice[39] were a kind gift of Meng Li (MRC Clinical Science Center). *Pitx3-Cre* mice[93] were a kind gift from Marten Smidt (University of Amsterdam). The genotype of *Pitx3-GFP* animals was determined by detection of fluorescence signal (in the retina). For all samples, heterozygous animals from WT mothers and homozygous fathers were used. The *Pitx3-ITC* mouse line was generated and reported previously[10]. Fluorescent signal was induced by breeding with *ACTB-FlpE* mice[94]. For *Pitx3-ITC;ACTB-FlpE* mice, genotyping was performed by PCR for Citrine, IFP and FlpE[10].

Immunohistochemistry

PFA-fixed embryonic (E12-E18) and postnatal (P0, P2, P3, P5, P10, P20) *Pitx3-ITC* brains or electroporated E18 *Pitx3-GFP* brains were cut into thick free-floating sections on a Leica VT1000S Vibratome (Leica Biosystems). For immunohistochemistry, sections were submerged in blocking buffer followed by primary antibody and secondary antibody incubation. Nuclei were stained with 4',6'-diamidino-2-phenylindole (DAPI, 0.1 mg/ml in 1x PBS; Invitrogen) and sections were mounted onto glass slides using FluorSave (Merck Millipore) or Mowiol 4-88 (#475904, Calbiochem). Primary antibodies used in this study include rabbit anti-RFP (1:1000, #600-401-379, Rockland), rabbit anti-TH (1:1000, #ab152, Millipore), sheep anti-TH (1:500-1:1000, #ab1542, Millipore), chicken anti-GFP (1:2000, #GFP-1020, AVES Labs) and chicken anti-GFP (1:1000, #13970 Abcam). Secondary antibodies used include Alexa fluor 488 Donkey anti-chicken (#703545155, Jackson Immunoresearch), Alexa fluor 555 donkey anti-sheep (#A21436, Lifetechnologies), Alexa fluor 568 donkey anti-rabbit (#ab175470, Abcam), Alexa Fluor 647 Donkey anti-sheep (#ab150179, Abcam). *Pitx3-ITC* timeline sections were imaged on a Zeiss LSM 880 Confocal Microscope. IUE samples were imaged on an AxioScope A1 epifluorescence microscope and analysed using Imaris software (version 8.4-9.4).

3DISCO brain clearing and FLSM

PFA-fixed E12, E13 and E15 whole embryos or E18 brains were subjected to a dehydration series with an increasing percentage of Methanol (MeOH). Samples were bleached overnight (ON). The following day, MeOH was removed stepwise and embryos were incubated in PBSGT blocking buffer and subsequently in primary

https://doi.org/10.1038/s41467-024-51041-1

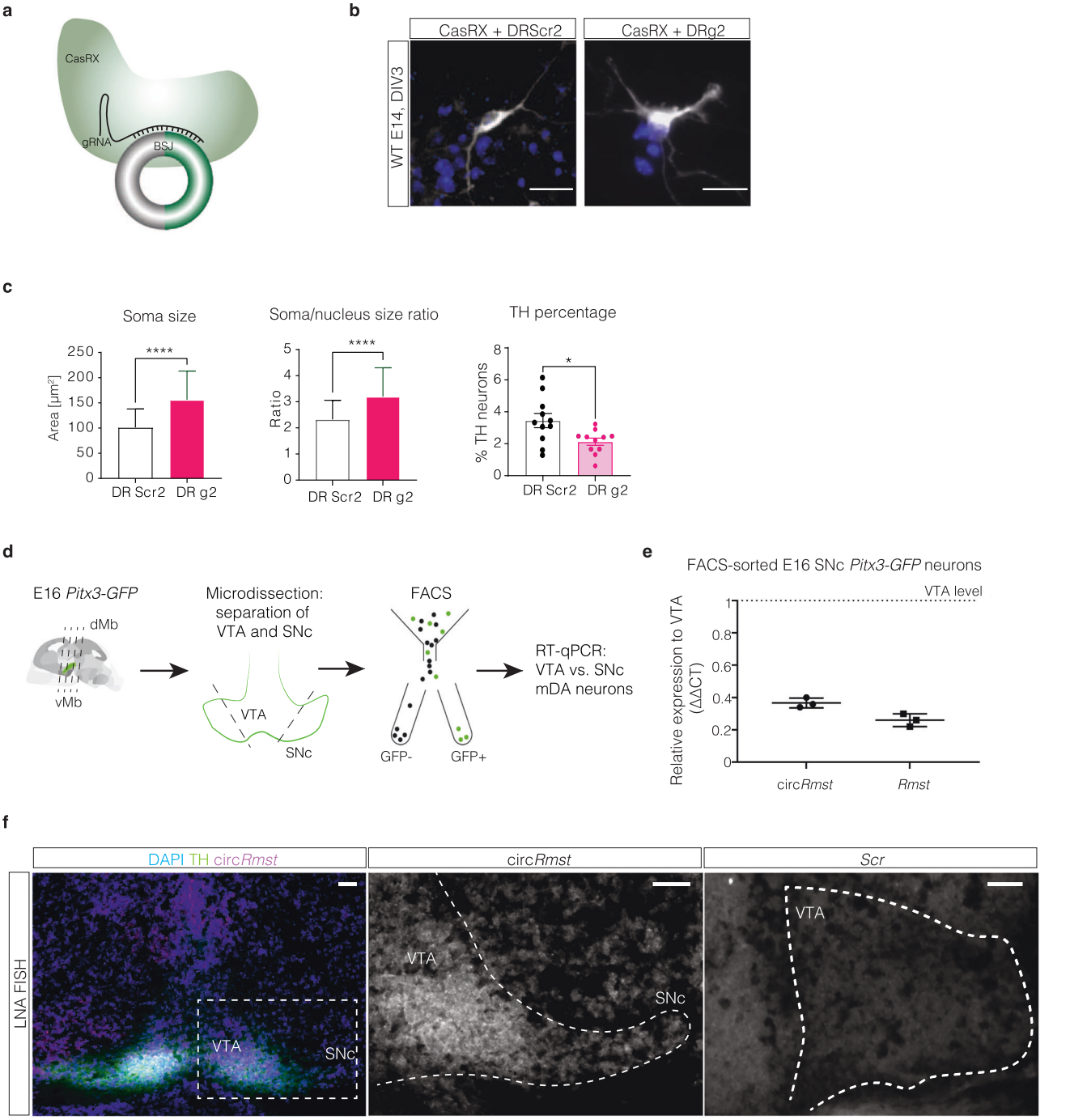

Fig. 7 | CasRx-mediated knockdown and VTA-enriched expression of circ*Rmst*. **a**–**c** circ*Rmst* KD induced by CasRx. **a** Schematic representation of CasRx-mediated KD. Guide RNA (gRNA) containing a CasRx recognition loop is directed to the BSJ of a circRNA. **b** Representative image of control (left) and CasRx-mediated circ*Rmst* KD (right) cultures at DIV3. TH = white, DAPI = blue, scale bars = 20 µm. **c** Quantification reveals an increase in soma size and soma-to-nucleus size ratio and a decrease in relative number of TH⁺ neurons. n = 50 (DR Scr2) & n = 75 (DR g2) for Soma size; n = 20 (DR Scr2) & n = 45 (DR g2) for Soma/Nucleus size ratio; n = 11 (DR Scr2) & n = 11 (DR g2) for TH percentage. Mean ± SD, normality with Shapiro-Wilk, unpaired two-tailed t-test, (soma size) ****$P < 0.0001$, (soma/nucleus) ****$P < 0.0001$, (TH percentage) *$P = 0.0154$. **d**, **e** Quantification of circ*Rmst* levels per subregion of the E16 mDA system. **d** Schematic representation showing dissection of E16 *Pitx3-GFP* brains into VTA and SNc regions followed by FACS sorting and RT-qPCR. **e** Quantification of the expression of circ*Rmst* and *Rmst* in subregions of the mDA neuron pool. n = 3 litters, mean ± SD, normality tested with Shapiro-Wilk, unpaired two-tailed t-test ****P = 0.0001. **f** LNA FISH for circ*Rmst* (and scrambled control) in cryosections of the E14 WT vMB. Boxed area is shown at higher magnification in the centre panel. Dashed lines in the two right panels indicate margin mDA neuron pool. circ*Rmst* expression is strongest in the VTA region. n = 3 brains. Scale bars = 50 µm. DIV days in vitro, WT wildtype, TH tyrosine hydroxylase, mDA midbrain dopamine, BSJ backsplice junction. Source data are provided as a Source Data file and Supplementary Data file.

antibody solution, followed by washes and secondary antibody incubation. Samples were dehydrated in tetrahydrofuran (THF) followed by removal of lipids by incubation in Dichlormethan. The final clearing step was performed by incubation in Dibenzylether (DBE). DBE was also used to match the refractive index (1.56) during imaging with an Ultramicroscope II light sheet microscope (LaVision BioTec) with a MVPLAPO 2x Objective lens (Olympus) and a Neo sCMOS camera (Andor; 2560×2160 pixels) and Imspector

https://doi.org/10.1038/s41467-024-51041-1

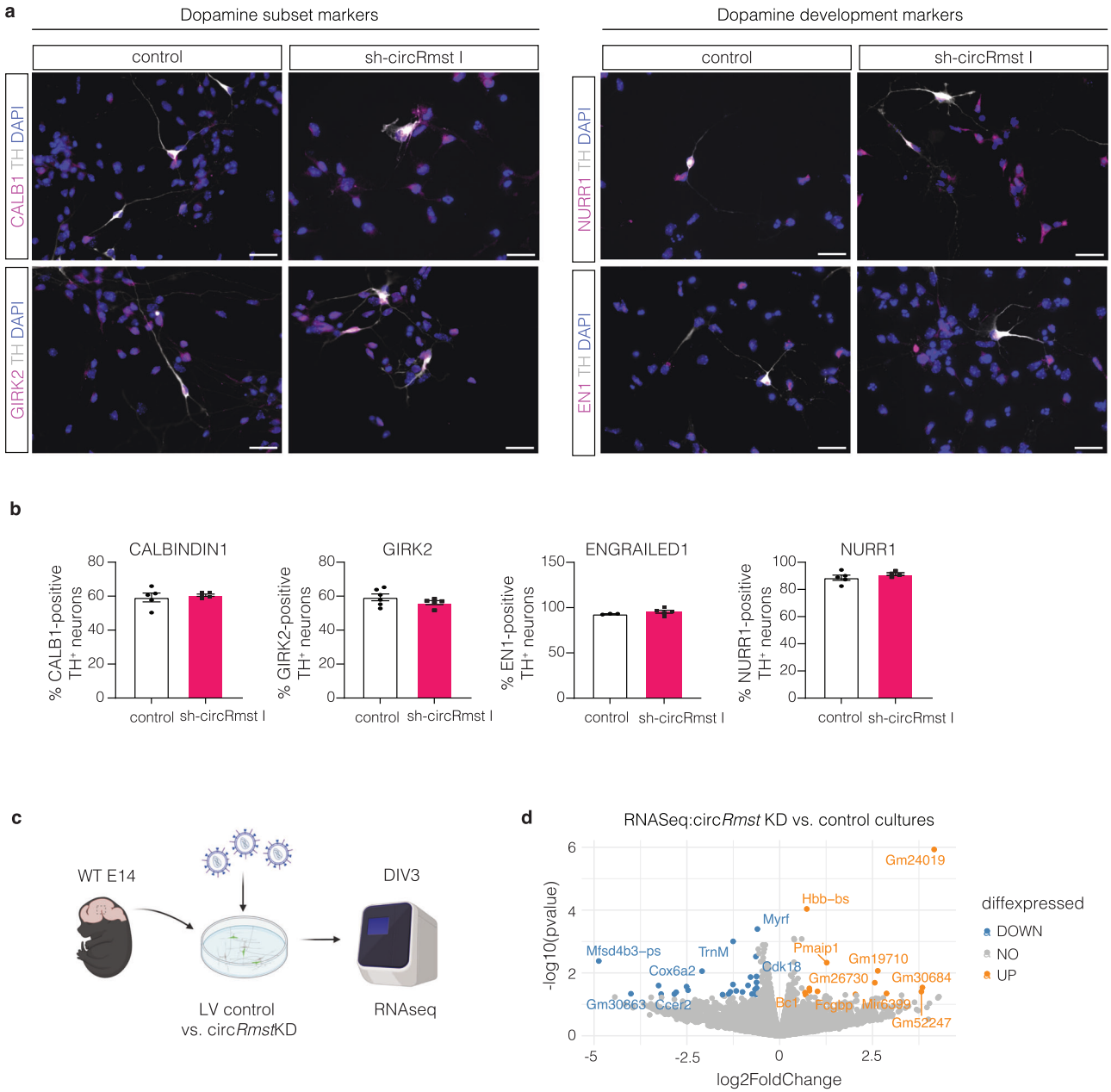

Fig. 8 | Characterisation of mDA cultures and transcriptomic profiling following circ*Rmst* KD. a, **b** mDA neuron subtype quantification following circ*Rmst* KD. **a** Representative image of control and circ*Rmst* KD cultures. **b** Quantification reveals no change in the relative cell count of the mDA subset markers CALB1 and GIRK2 and the mDA development markers NURR1 and EN1. CALB1: n = 5 (control) & n = 5 (shcircRmstI), GIRK2: n = 6 (control) & n = 5 (shcircRmstI), NURR1: n = 5 (control) & n = 4 (shcircRmstI), EN1: n = 3 (control) & n = 5 (shcircRmstI) primary vMB cultures. Scale bar = 25 μm. Data are presented as mean ± SEM, normality with Shapiro-Wilk, unpaired two-tailed t-test. **c** Schematic representation of circ*Rmst* knockdown (KD). Primary E14 WT vMB cultures were transduced with shRNA (or control) against the BSJ of circ*Rmst* (through lentiviral transduction) and subjected to RNAseq. Figure was generated with icons from BioRender.com. **d** Volcano plot of DEGs in RNAseq data following circ*Rmst* KD in E14 vMB cultures. Blue dots ($P < 0.05$, l2fc <-1) and orange dots ($P < 0.05$, l2fc > 1) represent DEGs. All RNAseq data statistics were performed with DESEq2 package. n = 3 cultures. TH tyrosine hydroxylase, CALB1 Calbindin1, GIRK1 G-protein-regulated inward-rectifier potassium channel, NURR1 Nuclear receptor related 1 protein, EN1 Engrailed1, DIV days in vitro, VTA ventral tegmental area, SNc substantia nigra pars compacta, RT-qPCR reverse transcription quantitative PCR, *Pitx3* Pituitary homeobox 3, LNA locked nucleic acid. Source data are provided as a Source Data file and Supplementary Data file.

software (version 5.0285.0; LaVision BioTech). 3D images were further analysed in Imaris (version 8.4-9.4).

Primary neuron collection and culture

The dissociation protocol was adapted and modified from literature[95,96]. E14, E16 and P0 *Pitx3*$^{GFP/+}$ mice were used for FACS purification, E14 and E11 WT embryos were used for primary vMB cultures. Micro-dissection of vMBs from *Pitx3*$^{GFP/+}$ mice was carried out under fluorescent light to visualise GFP$^+$ mDA neurons. Small tissue pieces were digested in Papain supplemented with DNase (LK003176 and LK003170, Worthington). After mechanical dissociation and purification over a BSA column, the cell pellet was recovered in either dissection medium for FACS or growth medium for culture. For RNAseq, micro-dissected vMBs of embryos from three (E14 RNAseq) or two (timeseries RNAseq) *Pitx3*$^{GFP/+}$ litters were used. To determine the expression levels of circ*Rmst* in the VTA and SNc, vMBs from three E16

https://doi.org/10.1038/s41467-024-51041-1

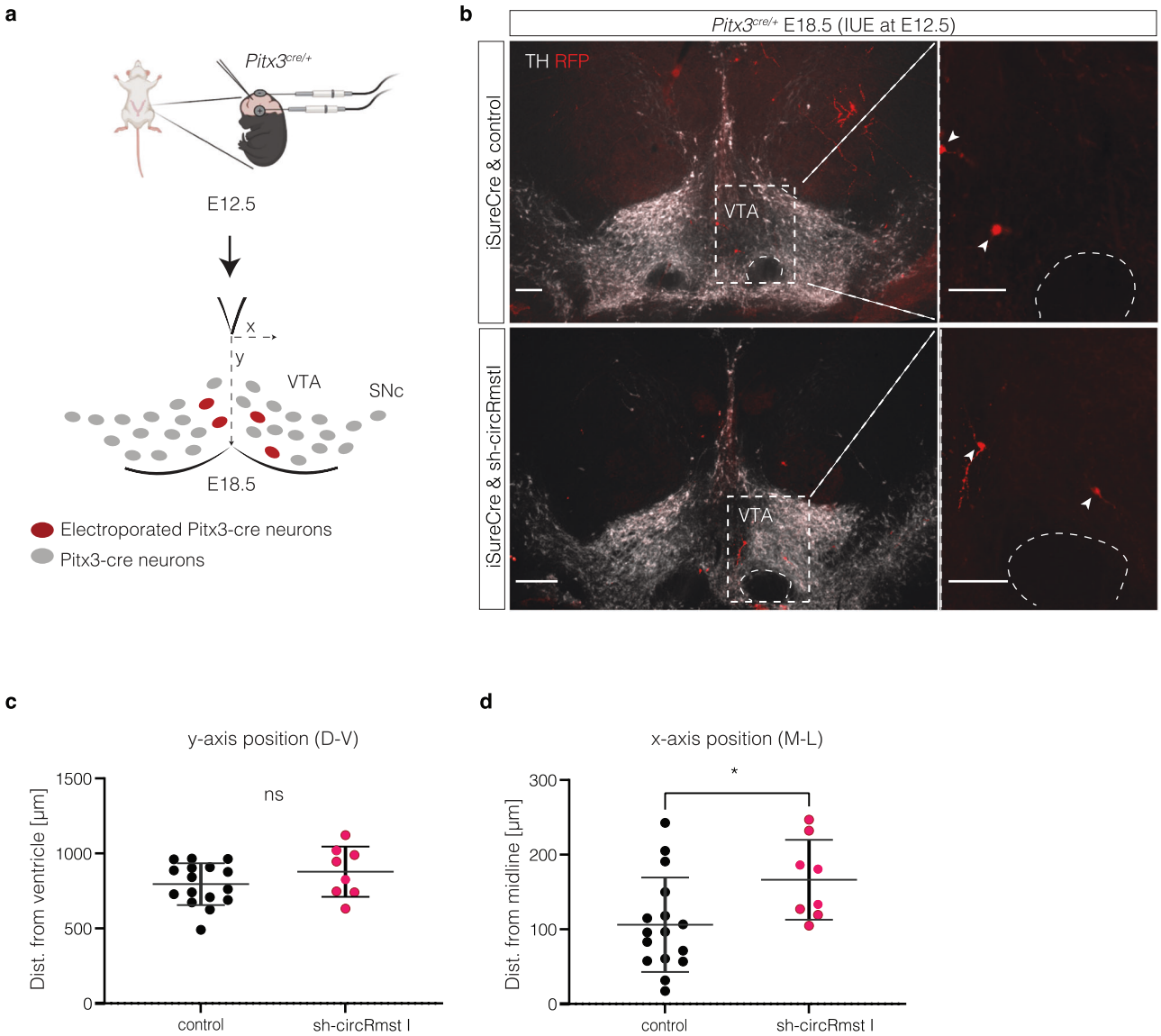

Fig. 9 | Analysis of mDA neuron positioning after in vivo circRmst knockdown. **a** Schematic representation of the IUE approach. Transuterine, intracerebroventricular injections with the Cre-dependent reporter *iSureCre* and a circ*Rmst* KD construct (*pll3.7-sh-circRmstl*) or control plasmid (*pll3.7-Scr2*) in the E12 vMB of *Pitx3*$^{cre/+}$ embryos were followed by transcranial vMB electroporation. At E18, brains were harvested and processed for immunohistochemistry. Figure was generated with icons from BioRender.com. **b** Representative images of electroporated mDA neurons in the E18 vMB after control or circ*Rmst* KD. White arrows indicate the position of electroporated mDA neurons. Boxed region is shown at higher magnification in right hand panels. circ*Rmst* KD causes neurons to migrate further away from the midline. Scale bars: left = 200 µm, right = 100 µm. **c**, **d** Quantification of the location of electroporated mDA neuron along the y- (dorsal-ventral) and x-axis (medial-lateral). Datapoints represent average per brain. n (*pll3.7)* = 16 brains, n (*pll3.7-sh-circRmstl)* = 8 brains, paired two-tailed t-test, mean ± SD, (**c**) *P* = 0.2529 (**d**) **P* = 0.0264. IUE *in utero* electroporation, D dorsal, L lateral, M medial, V ventral. Source data are provided as a Source Data file.

Pitx3$^{GFP/+}$ litters were micro-dissected. Tissue from VTA or SNc was dissociated in parallel.

For cultures, E14 and E11 WT vMBs were harvested and dissociated as described. 120,000–150,000 cells were plated as a drop on each precoated (poly-L-Ornithine (50 µg/ml, #P3655, Sigma), Laminin (10 µg/ml, #11243217001, Roche)) coverslip in a 24-well plate (Corning). Cells were counted on a Countess II FL automated cell counter (ThermoFisher). After 45–60 min of incubation at 37 °C/5% CO_2, 500 µl complete growth medium was added to the pre-incubated drops. The day after plating, half of the medium was replaced.

Fluorescence-activated cell sorting (FACS)

Shortly before sorting, DAPI was added to each sample for live cell gating. Cells were sorted with an 85 µm nozzle, directly collected in Qiazol (#79306, Qiagen) and frozen immediately on dry ice. After selection for singlets, cells were first gated for viability based on DAPI uptake, followed by selection of *Pitx3-GFP*$^{+}$ cells. Gating was kept consistent for all experiments. The cell sorts were carried out on a BD FACS Aria II Flow Cytometer.

RNA extraction, cDNA synthesis and RT-qPCR

RNA for RT-qPCR from sorted neurons and vMB circRNA KD cultures was extracted using the miRNeasy micro kit (#217084, Qiagen) and miRNeasy mini kit (#217004, Qiagen), respectively. The manufacturer's recommendations were followed including on-column DNAse treatment (#79254, Qiagen) and the addition of 2-propanol to RWT buffer. SuperScript IV Reverse Transcriptase kit (#18090010, Thermo Fisher) was used to generate cDNA using 500 ng isolated RNA.

https://doi.org/10.1038/s41467-024-51041-1

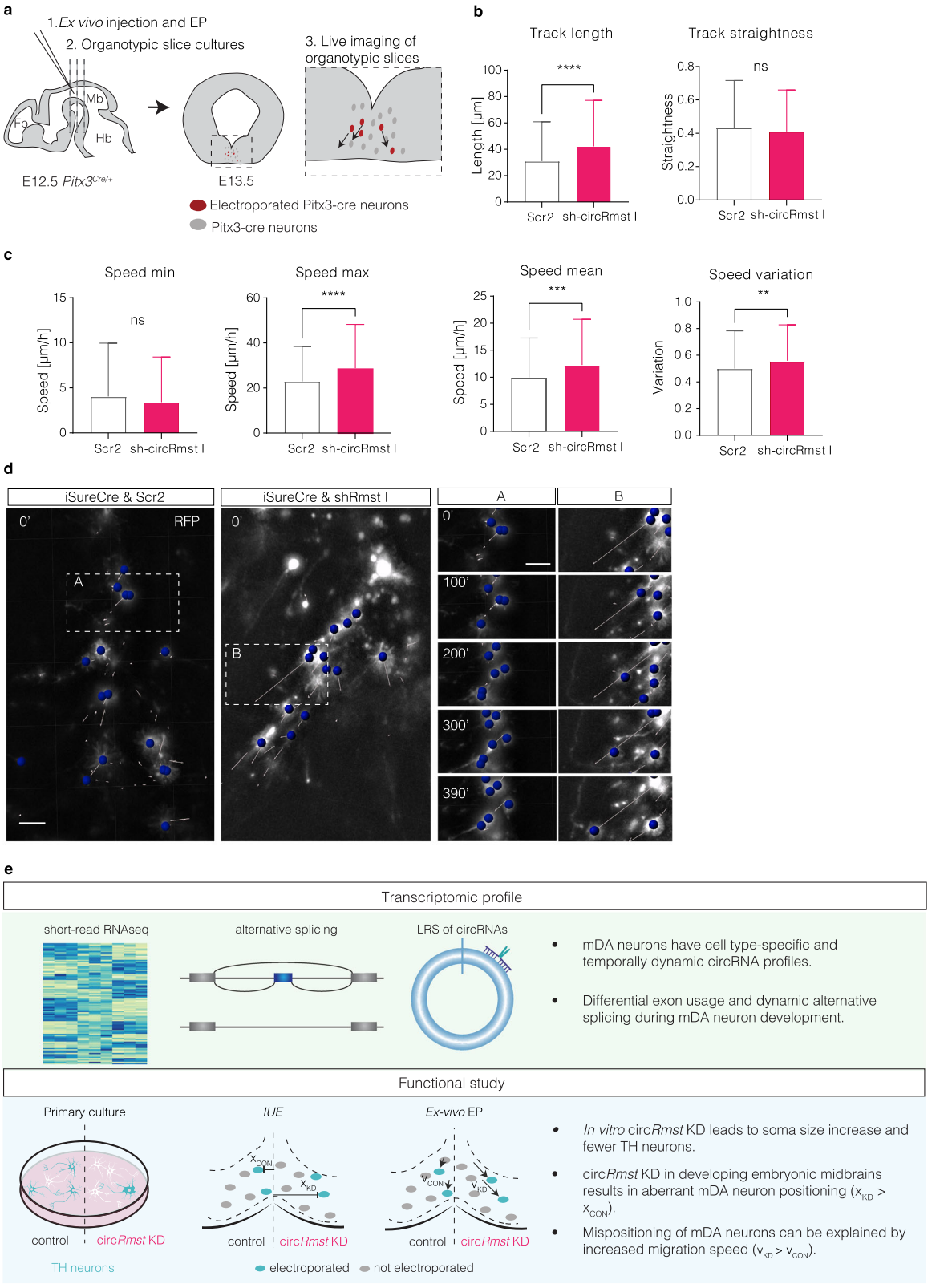

For primary culture lysates, RNA amount was adjusted to that of the lowest concentration in the experiment. *C. elegans*-derived RNA was added as spike-in. circRNAs were quantified using divergent, BSJ-amplifying primers. RT-qPCRs were run in a QuantStudio 6/7 Flex System qPCR cycler (Applied Biosystems). The 2^-ddCT method was used to calculate for relative expression. *Rpl13a* and *Tbp* were used as housekeeping genes. For relative comparison, normalisation to cell type (GFP^+ vs. GFP^-) or control samples (e.g. Scr vs. sh-circRmst) was performed and control values were set to 1.

For miRNA RT-qPCRs, the miRCURY LNA miRNA PCR Assay (#YP00204762, Qiagen) was used according to manufacturer's protocol. Primers were designed to detect *hsa-miR-135a-5p* (miRbase ID: MIMAT0000428). Primers targeting the U6 spike-in and 5S were used as technical and internal controls, respectively.

Fig. 10 | Analysis of mDA neuron migration parameters following ex vivo circ*Rmst* knockdown. a Schematic representation of the ex vivo electroporation and analysis of organotypic slice cultures. Intracerebroventricular injection (*iSureCre* and *pll3.7-sh-circRmstI* or *pll3.7-Scr2*) and vMB electroporation of E12 *Pitx3*$^{cre/+}$ embryonic brains followed by live imaging of DIV1 organotypic slice cultures. **b**, **c** Quantification of electroporated mDA neurons (RFP$^+$). Slices were subjected to circ*Rmst* KD and control cultures were analysed for (**b**) track length, track straightness and (**c**) minimum (min), maximum (max) and mean speed, and speed variation. n = 3 cultures (analysis of 326 neurons for Scr2 and 404 neurons for sh-circRmstI), unpaired two-tailed t-test, mean ± SD, (**b**) ****$P = 0.0001$, $P = 0.2606$, (**c**) $P = 0.1086$, ****$P = 0.0001$, ***$P = 0.0002$, **$P = 0.0050$. **d** Representative images of electroporated organotypic slice cultures at different timepoints during recording in control (left) and circ*Rmst* KD (centre) experiments. Blue spheres indicate detected neurons. Trajectory directions are shown as white arrows. Scale bars = 40 μm. Experiment was carried out using 3 cultures (analysis of 326 neurons for Scr2 and 404 neurons for sh-circRmstI). **e** Graphical summary of this study. (Top) Transcriptomic profiling and alternative splicing analysis of developing mDA neurons identify novel cell type-specific and dynamic expression and regulation of circRNAs. (Bottom) Circ*Rmst* regulates mDA neuronal morphology and neuron number in vitro, and is required for proper migration of these neurons in vivo by controlling migration speed. *Pitx3* Pituitary homeobox 3, Fb forebrain, Mb midbrain, Hb hindbrain, LRS long-read sequencing. Source data are provided as a Source Data file.

Sequencing of the circ*Rmst* BSJ

Sequencing of circRNA BSJ was performed as previously described[97], with minor modifications. RT-qPCR was performed to amplify the BSJ using specific circ*Rmst* BSJ primers. For each circRNA candidate, RT-qPCR was performed in five replicates. RT-qPCR reactions were pooled and separated on an Agarose gel. Excised bands were purified (PureLink™ Quick Gel Extraction Kit, #K210012, Invitrogen) and subjected to Sanger sequencing (Macrogen).

Short-read RNA sequencing and analysis

For RNAseq, RNA of sorted cells was extracted using the miRNeasy micro kit (#217084, Qiagen), followed by rRNA depletion (riboZero, Illumina). Sequencing libraries were generated by applying Script-Seq v2 (Illumina). Raw data was filtered, trimmed and analysed using trim_galore, Tophat2[98] and DESeq2[40]. CircRNA discovery was performed with find_circ[31] and CIRCexplorer[44] (E14 *Pitx3-GFP*$^+$ versus GFP) or CIRI2[47] and CIRCexplorer2[48] (timeseries E14, E16 and P0 *Pitx3-GFP*$^+$). CircRNA detection was run on individual samples and combined using a modified version of CircM. For identification, results were compared to CIRCpedia[48], circBase[99] and circAtlas[100] databases. Due to availability of novel tools, different identification pipelines were used as compared to the E14 RNAseq. Comparison of BSJ prediction (baseMean > 1) at E14 using the primary tools revealed that all circRNAs identified by find_circ were detected by CIRI2. Due to a higher number of total circRNAs detected in CIRI2, the vice versa comparison overlapped by ca. 35%. Differential exon usage was analysed with DEXseq[46].

For RNAseq on cultures following KD, E14 WT vMB cultures were prepared (150,000 cells per well) and transduced (lentivirus expressing *pll3.7-Scr2* or *pll3.7-shRmstI* (MOI5)) as described above. At 3 DIV, 2–3 wells per sample were pooled in Qiazol and stored at −80 °C until processing. RNA was extracted using miRNeasy mini kit (Qiagen). KD of each sample was confirmed by RT-qPCR in a technical duplicate. Library preparation and Illumina NovaSeq6000 sequencing (Paired-End, 150 bp.) was performed at Genome Scan (Leiden). Per sample ~18 Gb, 60 million paired-end reads were obtained. Differential expression was analysed with DESeq2. Raw and processed RNAseq data is deposited at NCBI Gene Expression Omnibus (GEO) with accession numbers GSE229481 for timeseries and GSE229486 for KD samples.

Long-read sequencing of circRNA and analysis

ONT sequencing was performed as described previously[52], with modifications to allow for low RNA input. Briefly, a panel of 25 circRNAs was composed from our short-read sequencing data and literature. Extended divergent primers with 25 circRNA-specific nucleotides, were designed for each circRNA, compatible with ONT barcoded PCR primers (ONT kit, #SQKPCB109) (Supplementary Data 3). cDNA synthesis was performed using Maxima H Minus Reverse Transcriptase (Thermo Fisher Scientific, EP0752). Total RNA was *DNase* I treated and RNA-Primer mix, 5x RT Buffer and RiboLock *RNase* inhibitor, RT enzyme and *RNase* H (Thermo Fisher Scientific, #EN0201) and *RNase* Cocktail Enzyme Mix (Thermo Fisher Scientific, #AM2286) were added to the sample.

The second cDNA strand was synthesised by the addition of second strand cDNA synthesis primer mix and LongAmp Hot Start Taq 2X Master Mix (New England Biolabs, #M0533L). Unincorporated primers were digested using Exonuclease I (New England Biolabs, M0293S) and PCR products were cleaned using SPRIselect beads. Later, the library prep and PCR reaction were subjected to PCR with barcoded cPRM primers from the SQK-PCB109 kit following the provided manual by the manufacturer. After Exonuclease I treatment, purified libraries were cleaned using SPRISelect beads and eluted elution buffer. Qubit 4 (ThermoFisher), 2100 bioanalyzer (Agilent) and Nanodrop (ThermoFisher) were used to assess the quantity, quality and purity. Equimolar ratios of libraries were pooled and multiplexed for adaptor ligation and ONT MinION sequencing, following the manufacturer's instructions.

Basecalling and demultiplexing was done using Guppy (version 5.0.11+2b6dbff). For quality filtering, genome mapping, circRNA detection quantification and annotation, the following tool was used: https://github.com/omiics-dk/long_read_circRNA. The circPanel-LRS data was analysed as described previously[52], focusing on full length circRNA sequence discovery. Parameters for circRNA sequence discovery and analysis of coverage were adapted to the error rate of ONT sequencing. To analyse AS events, different cut-offs of the maximum coverage (10%, 30%) were applied. ONT circRNA sequencing data is available at the Gene Expression Omnibus (GEO) with accession number GSE229597.

Alternative splicing analysis

Illumina sequencing data of E14 *Pitx3-GFP*$^+$ versus GFP$^-$ and timeseries (E14, E16, P0 *Pitx3-GFP*$^+$) were mapped to the mouse genome (mm10) using Tophat2. Alternative splicing (AS) was detected using rMATS[42] (v4.1.1), using Gencode gene annotations M19. Differential AS events were found for relevant groups by rMATS. Analysis and overview figures were made in R. Volcano plots (−log10(FDR)) vs ΔPSI (difference in percent spliced-in) were generated for each AS event with FDR < 0.05. Violin plots illustrate the distribution of ΔPSI for each type of AS event where FDR < 0.05 and ΔPSI > 0.1. Sashimi plots visualise specific AS events and were generated with rmats2sashimiplot (v2.0.4).

Single molecule fluorescence in situ hybridisation (smFISH)

To visualise circRNAs in vitro, PFA-fixed DIV1 or DIV5 primary vMB cultures were subjected to smFISH. Custom made BSJ-spanning probes were used together with the ViewRNA miRNA cell kit (Thermo Fisher). Briefly, coverslips were crosslinked using Crosslinking buffer QM, followed by incubation in EDC solution. To permeabilise cells, coverslips were transferred to Detergent solution QC, followed by hybridisation with the probes (diluted in Probe set diluent QF). After thorough washes, Preamplifier mix QM (preamplification of the signal) and next Amplifier mix QM (amplification of the signal) were applied. After repeating the washing steps, Working Label Probe Mix Solution was used to label the target. The fluorescent signal was developed by

application of AP Enhancer solution and fresh Fast red substrate. Finally, coverslips were washed, post-fixed and immunolabelling was performed as described.

Locked nucleic acid fluorescence in situ hybridisation (LNA-FISH)

LNA-FISH was performed as described previously[101]. Briefly, 20 mm sections of E14 WT midbrains were pre-fixed, acetylated and permeabilized with proteinase K. Prehybridization with hybridisation buffer was followed by overnight hybridisation with a custom made 3' and 5' DIG-labelled probe against the BSJ of circ*Rmst* (Sequence: AACCTGAGTATCTCATGAAGCC, Qiagen) or a scrambled control (Qiagen). The next day, sections were washed and incubated in 0.2x SSC followed with washes in B1 solution supplemented with Tween. For immunohistochemistry and ISH, slides were blocked in 10% FBS in B1 buffer with Tween and subsequently incubated with anti-DIG-POD (1:500; Roche Diagnostics; Cat. #11207733910) and rabbit anti-TH (1:500, #ab152, Millipore) antibodies. The next day, sections were incubated with TSA™ Cyanine 3 reagent (1:50 in amplification diluent; #SAT704A001EA, AKOYA Biosciences) followed by incubation with secondary antibody goat-anti-rabbit-Alexa 488 (1:500; Invitrogen). Finally, DAPI was used to visualise nuclei. Slides were mounted with FluorSave™ reagent (Millipore) and images were acquired on an epifluorescence microscope (Zeiss) with image acquisition software (Zen 3.3, Zeiss).

Plasmid cloning

To specifically knockdown circ*Rmst*, circ*Ezh2*, circ*Lmx1a*, circ*Fat3*, circ*Gigyf2* and circ*Tulp4*, shRNA-mediated KD was performed. Additionally, for circ*Rmst* a CasRx/gRNA-mediated KD approach was developed. For each approach, three BSJ-targeting sequences were designed (shcirc*Ezh2/Fat3/Gigyf2/Lmx1a/Rmst/Tulp4* I-III and circ*Rmst* DRgRNA 1-3, respectively). shRNA designs included the biosettia loop (https://biosettia.com/support/shrna-designer/seqreview/) between two 21 nt long BSJ-targeting sequences. For the gRNAs, a recognition motif for CasRx (DR) was included. *pLentiLox3.7* (*pll3.7*) was used as a backbone for shRNAs and gRNAs and was a gift from Luk Parijs (#11795, Addgene). The backbone was restricted with *Xho*I (#10899194001, Roche) and *Hpa*I (#10380385001, Roche) in Cut Smart buffer (#B7204, NEB). Annealed oligonucleotides were ligated using T4 Ligation Buffer (Roche), ATP, T4 Polynucleotide Kinase (#M0201, NEB) and T4 DNA ligase (#10799009001, Roche). One Shot chemically competent Stbl3 (#C737303, ThermoFisher) were used for transformation according to the manufacturer's protocol. Colonies were selected on carbenicillin or ampicillin plates. Sanger sequencing was performed to validate positive clones.

Lentivirus production

HEK293T cells (#CRL-11268, ATCC) were transfected with a lentivector (*pll3.7*, *pll3.7-Scr2*, *pll3.7-shcircRNA* (*Ezh2/Fat3/Gigyf2/Lmx1a/Rmst/Tulp4*), *pll3.7-DRgRNA2* or *pXR001: EF1a-CasRx-2A-EGFP* (CasRx; #109049, Addgene)) and virus helper- and packaging plasmids *pMD2.G-VSVG* (#12259, Addgene), *psMDLg/pRRE* (#12251, Addgene) and *pRSV-Rev* (#12253, Addgene). *pMD2.G-VSVG*, *pMDLg/pRRE* and *pRSV-Rev* were a gift from Didier Trono[102]. 48-72 h post-transfection, virus was harvested from the media by ultracentrifugation. Lentivirus pellets were dissolved in 0.5% BSA in 1x PBS, aliquoted and stored at −80 °C until use. The titre was determined by quantification of fluorescent cells in a virus dilution series or by using the Lenti Go Stix (#631280, Takara) titre tests.

Knockdown in primary mDA cultures

vMBs from one litter of E14 or E11 WT embryos were dissociated and plated as described previously. For KD experiments, 120,000–150,000 cells were plated as a drop on each pre-coated coverslip. The cultures were transduced with lentivirus (*pll3.7-/pll3.7-Scr2/pll3.7-shRNA--circRNA (Ezh2/Fat3/Gigyf2/Lmx1a/Rmst/Tulp4)* (MOI5) or *CasRx* and *pll3.7-DRScr2/pll3.7-DRgRNA2* (MOI5 each)) on DIV1 (shRNA design test) or on the day of plating (all further experiments). Three days post-infection, DIV3 and DIV4, cells were fixed in PFA for morphological analysis or RNA was harvested using Qiazol, respectively. For RT-qPCR, 2–3 wells of the same condition were pooled per sample. circRNA KD was confirmed in duplicates by RT-qPCR prior to each morphological analysis.

KD cultures were fixed and stained with rabbit anti-TH (1:1000, #ab152; Millipore), mouse anti-TH (1:300, #MAB318; Sigma-Aldrich), mouse anti-Calb1 (1:500, #C9848; Sigma), Rabbit anti-Girk2 (1:500, #APC-006, Alomone Labs), Rabbit anti-Nurr1 (1:10–1:20, #PA5-13416; Invitrogen), Rabbit anti-En1 (1:100, #BS-11744R; Bioss), or chicken anti-GFP (1:1000, #GFP-1020; Aves Labs). For fluorescent labelling, secondary antibodies Alexa Fluor 488 Donkey anti-chicken (1:500–1:750, #703-545-155, Jackson Immuno Research), Alexa Fluor 568 Donkey anti-mouse (1:500–1:750, #A10037; Invitrogen), Alexa Fluor 568 Donkey anti-rabbit (1:500–1:750, #ab175470; Abcam), Alexa Fluor 647 Donkey anti-mouse (1:500–1:750, #A-31571; Invitrogen), Alexa Fluor 647 Donkey anti-Rabbit (1:500–1:750, #A32795; Thermo Scientific), Alexa Fluor 488 Goat anti-rabbit (1:750, #Ab150077; Abcam), Alexa Fluor 568 Goat anti-mouse (1:750, #A11004; Thermo Scientific), Alexa Fluor 647 Goat anti-chicken (1:750, #A21449; Invitrogen) and Alexa Fluor 488 Goat anti-chicken (1:750, #Ab150169; Abcam) were applied. Coverslips were incubated with DAPI (Sigma-Aldrich) and mounted on microscopy glass slides with FluorSave (Merck Millipore). shRNA KD cultures were imaged on a Zeiss LSM880 confocal microscope (40x) for morphology, on a Zeiss AxioImager M2 epifluorescence microscope (20x tiled) for estimating mDA neuron marker % and on a Zeiss AxioScope A1 epifluorescence microscope (10x) for TH%. CasRx-KD culture imaging was performed on an AxioImager M2 epifluorescent microscope (20x and 10x). Images were analysed in FIJI.

In utero electroporation

E12 *Pitx3*$^{cre/+}$ embryos were subjected to IUE. Embryos were exposed by a laparotomy to the pregnant mother and intracerebroventricularly injected with a mix comprising 1 μg/μl shRNA plasmid (*pll3.7-shRmstI* or *pll3.7-Scr2*), 0.5 μl *iSureCre*[60] and FastGreen in physiological saline. *iSureCre* was a gift from Rui Benedito (CNIC). The electrodes were positioned to pull the plasmid towards the vMB and fired with 30 V for 50 ms, 5 times with an interval of 950 ms. Subsequently, embryos were placed back into the abdomen. Embryonic brains were harvested at E18 for further analysis.

Ex vivo electroporation

E12 *Pitx3*$^{cre/+}$ embryos were extracted from the uterus and injected intracerebroventricularly with a plasmid mix containing 0.5 μg/μl *iSureCre*[60], 1 μg/μl *pll3.7-shRmstI* or *pll3.7-Scr2* and FastGreen in physiological saline. Electroporation was performed with eight pulses of 40 V for 50 ms in a 950 ms interval. Subsequently, organotypic slice cultures were prepared as described previously[103], with modifications. Briefly, brains were embedded in 4% low melting agarose (m/v) in supplemented HBSS and cut on a Leica vibratome. Midbrain sections of 250 μm were collected on ice in cell culture inserts (#PICMORG50, Millipore), transferred into a plate containing pre-warmed slice culture medium (Basal Medium Eagle (Sigma) with cHBSS, glucose, glutamine and P/S) and incubated ON at 37 °C. At DIV1, slices were imaged on a Leica Thunder microscope using a 10x objective. After thunder computational clearing was applied, images were analysed in Imaris.

Secondary structure prediction

To predict the secondary structures of circ*Rmst*, the RNAfold webserver was used[104].

RBP and miRNA prediction

Potential interaction partners of circ*Rmst* were detected using RBPmap (RBPs) or mirDB (miRNAs). The resulting gene lists were analysed for associated pathways (Panther[105]).

Statistical information

RNAseq data (E14 GFP$^+$ versus GFP$^-$, GFP$^+$ timeseries and circ*Rmst* KD) were analysed with DESeq2 using R. *P* values and adjusted *P*-values (padj) for each gene are indicated in Supplementary Data 1–3. *P*adj < 0.05 was considered significant. For AS analysis, rMATS was used, significance is indicated by FDR. Parameters of neuronal morphology (e.g. soma size, neurite number, neurite length) upon circRNA KD in E11 (circ*Rmst*) and E14 (circ*Rmst*, circ*Fat3*, circ*Ezh2*, circ*Tulp4*) cultures were analysed using two-tailed unpaired t-tests or two-tailed Mann Whitney U-tests in Prism Graphpad (30-90 neurons per condition were analysed in 3–4 cultures). smFISH data was analysed with multiple unpaired t-tests with Holm Sidak multiple testing (n = 2–3 cultures) or ordinary one-way ANOVA with Tukey's multiple comparisons test (n = 3–4 cultures), respectively. Multiple t-tests were used for analysing the Sholl analysis in E14 cultures. Neuron position after IUE was analysed using two-tailed unpaired paired t-test (n=averages of 16 control brains and 8 circ*Rmst* KD brains). Neuron migration (ex vivo electroporation) was analysed using a two-tailed unpaired t-test (n = 3 slice cultures). *Rmst* isoform expression was analysed using one-way ANOVA. *RNase* R resistance of circ*Rmst* was analysed with multiple t-tests (n = 5). RT-qPCRs for KD validations, control versus shRNA designs and Scr2 vs. shRNA/ CasRx were analysed with multiple t-tests (n = 3) and paired t-test (n = 3), respectively. *MiR-135a* levels upon circ*Rmst* KD were analysed using paired t-test (n = 4). Where statistical significance was indicated with asterisks, following classification was used: $^*P < 0.05$, $^{**}P < 0.01$, $^{***}P < 0.005$, $^{****}P < 0.001$. Detailed sample numbers (n) and p-values are listed in the corresponding figure legends.

Reporting summary

Further information on research design is available in the Nature Portfolio Reporting Summary linked to this article.

Data availability

The data supporting the findings of this study are available from the corresponding authors upon request. Raw and processed RNAseq data is deposited at NCBI Gene Expression Omnibus (GEO) with accession numbers GSE229481 for timeseries (short-read RNAseq), GSE229486 for KD samples (short-read RNAseq) and GSE229597 for ONT circRNA sequencing data. Source data are provided with this paper.

References

1. Garritsen, O., van Battum, E. Y., Grossouw, L. M. & Pasterkamp, R. J. Development, wiring and function of dopamine neuron subtypes. *Nat. Rev. Neurosci.* 1–19. https://doi.org/10.1038/s41583-022-00669-3 (2023).
2. Björklund, A. & Dunnett, S. Dopamine neuron systems in the brain: an update. *Trends Neurosci.* **30**, 194–202 (2007).
3. Arenas, E., Denham, M. & Villaescusa, J. C. How to make a midbrain dopaminergic neuron. *Development* **142**, 1918–1936 (2015).
4. Cardoso, T. & Lévesque, M. Toward generating subtype-specific mesencephalic dopaminergic neurons in vitro. *Front. Cell Dev. Biol.* **0**, 443 (2020).
5. Islam, K. U. S., Meli, N. & Blaess, S. The development of the mesoprefrontal dopaminergic system in health and disease. *Front. Neural Circuits* **15**, 746582 (2021).
6. Xu, B. et al. Critical roles for the netrin receptor deleted in colorectal cancer in dopaminergic neuronal precursor migration, axon guidance, and axon arborization. *Neuroscience* **169**, 932–949 (2010).
7. Yang, S. et al. Cxcl12/Cxcr4 signaling controls the migration and process orientation of A9-A10 dopaminergic neurons. *Dev. (Camb.)* **140**, 4554–4564 (2013).
8. Bodea, G. O. et al. Reelin and CXCL12 regulate distinct migratory behaviors during the development of the dopaminergic system. *Development* **141**, 661–673 (2014).
9. Vaswani, A. R. et al. Correct setup of the substantia nigra requires reelin-mediated fast, laterally-directed migration of dopaminergic neurons. *Elife* **8**, e41623 (2019).
10. Brignani, S. et al. Remotely produced and axon-derived netrin-1 instructs GABAergic neuron migration and dopaminergic substantia nigra development. *Neuron* https://doi.org/10.1016/j.neuron.2020.05.037 (2020).
11. Poulin, J. F. et al. Defining midbrain dopaminergic neuron diversity by single-cell gene expression profiling. *Cell Rep.* https://doi.org/10.1016/j.celrep.2014.10.008 (2014).
12. Tiklová, K. et al. Single-cell RNA sequencing reveals midbrain dopamine neuron diversity emerging during mouse brain development. *Nat. Commun.* https://doi.org/10.1038/s41467-019-08453-1 (2019).
13. Hook, P. W. et al. Single-cell RNA-seq of mouse dopaminergic neurons informs candidate gene selection for sporadic parkinson disease. *Am. J. Hum. Genet.* https://doi.org/10.1016/j.ajhg.2018.02.001 (2018).
14. Poulin, J.-F. F., Gaertner, Z., Moreno-Ramos, O. A. & Awatramani, R. Classification of midbrain dopamine neurons using single-cell gene expression profiling approaches. *Trends Neurosci.* **43**, 155–169 (2020).
15. La Manno, G. et al. Molecular diversity of midbrain development in mouse, human, and stem cells. *Cell* https://doi.org/10.1016/j.cell.2016.09.027 (2016).
16. Gendron, J. et al. Long non-coding RNA repertoire and open chromatin regions constitute midbrain dopaminergic neuron-specific molecular signatures. *Sci. Rep.* **9**, 1–16 (2019).
17. Salvatori, B., Biscarini, S. & Morlando, M. Non-coding RNAs in nervous system development and disease. *Front. Cell Dev. Biol.* **8**, 273 (2020).
18. Rajman, M. & Schratt, G. MicroRNAs in neural development: from master regulators to fine-tuners. *Development* **144**, 2310–2322 (2017).
19. Vangoor, V. R., Gomes-Duarte, A. & Pasterkamp, R. J. Long non-coding RNAs in motor neuron development and disease. *J. Neurochem* **156**, 777–801 (2021).
20. Nielsen, A. F. et al. Best practice standards for circular RNA research. *Nat. Methods* 1–13. https://doi.org/10.1038/s41592-022-01487-2 (2022).
21. Mattick, J. S. et al. Long non-coding RNAs: definitions, functions, challenges and recommendations. *Nat. Rev. Mol. Cell Biol.* **17**, 1–17 (2023).
22. Feng, Z., Zhang, L., Wang, S. & Hong, Q. Circular RNA circDLGAP4 exerts neuroprotective effects via modulating miR-134-5p/CREB pathway in Parkinson's disease. *Biochem. Biophys. Res. Commun.* https://doi.org/10.1016/j.bbrc.2019.11.102 (2020).
23. Jia, E. et al. Transcriptomic profiling of circular RNA in different brain regions of Parkinson's disease in a mouse model. *Int. J. Mol. Sci.* **21**, 3006 (2020).
24. Dong, X. et al. Circular RNAs in the human brain are tailored to neuron identity and neuropsychiatric disease. *Nat. Commun.* **14**, 1–12 (2023).
25. Cai, L. et al. Downregulation of lncRNA UCA1 ameliorates the damage of dopaminergic neurons, reduces oxidative stress and inflammation in Parkinson's disease through the inhibition of the

PI3K/Akt signaling pathway. *Int. Immunopharmacol.* **75**, 105734 (2019).
26. Venø, M. T. et al. Spatio-temporal regulation of circular RNA expression during porcine embryonic brain development. *Genome Biol.* **16**, 245 (2015).
27. Pascale, E. et al. Noncoding RNAs and midbrain DA neurons: novel molecular mechanisms and therapeutic targets in health and disease. *Biomolecules* **10**, 1–21 (2020).
28. Gruhl, F., Janich, P., Kaessmann, H. & Gatfield, D. Circular RNA repertoires are associated with evolutionarily young transposable elements. *Elife* **10**, e67991 (2021).
29. Ashwal-Fluss, R. et al. CircRNA Biogenesis competes with Pre-mRNA splicing. *Mol. Cell* **56**, 55–66 (2014).
30. Hansen, T. B. et al. Natural RNA circles function as efficient microRNA sponges. *Nature* https://doi.org/10.1038/nature11993 (2013).
31. Memczak, S. et al. Circular RNAs are a large class of animal RNAs with regulatory potency. *Nature* https://doi.org/10.1038/nature11928 (2013).
32. Salzman, J. Circular RNA expression: its potential regulation and function. *Trends Genet.* **32**, 309–316 (2016).
33. Rybak-Wolf, A. et al. Circular RNAs in the mammalian brain are highly abundant, conserved, and dynamically expressed. *Mol. Cell* https://doi.org/10.1016/j.molcel.2015.03.027 (2014).
34. You, X. et al. Neural circular RNAs are derived from synaptic genes and regulated by development and plasticity. *Nat. Neurosci.* **18**, 603–610 (2015).
35. Zimmerman, A. J. et al. A psychiatric disease-related circular RNA controls synaptic gene expression and cognition. *Mol. Psychiatry* 1–16. https://doi.org/10.1038/s41380-020-0653-4 (2020).
36. Suenkel, C., Cavalli, D., Massalini, S., Calegari, F. & Rajewsky, N. A highly conserved circular RNA is required to keep neural cells in a progenitor state in the mammalian brain. *Cell Rep.* **30**, 2170–2179.e5 (2020).
37. Seeler, S. et al. A circular RNA expressed from the FAT3 locus regulates neural development. *Mol. Neurobiol.* https://doi.org/10.1007/s12035-023-03253-7 (2023).
38. Crittenden, J. R. et al. Striosome-dendron bouquets highlight a unique striatonigral circuit targeting dopamine-containing neurons. *Proc. Natl Acad. Sci. USA* **113**, 11318–11323 (2016).
39. Zhao, S. et al. Generation of embryonic stem cells and transgenic mice expressing green fluorescence protein in midbrain dopaminergic neurons. *Eur. J. Neurosci.* **19**, 1133–1140 (2004).
40. Love, M. I., Huber, W. & Anders, S. Moderated estimation of fold change and dispersion for RNA-seq data with DESeq2. *Genome Biol.* **15**, 1–21 (2014).
41. Olthof, A. M., White, A. K. & Kanadia, R. N. The emerging significance of splicing in vertebrate development. *Development* **149**, dev200373 (2022).
42. Shen, S. et al. rMATS: robust and flexible detection of differential alternative splicing from replicate RNA-Seq data. *Proc. Natl Acad. Sci. USA* **111**, E5593–E5601 (2014).
43. Hansen, T. B. Improved circRNA identification by combining prediction algorithms. *Front. Cell Dev. Biol.* **6**, 330528 (2018).
44. Zhang, X.-O. O. et al. Complementary sequence-mediated exon circularization. *Cell* **159**, 134–147 (2014).
45. Ferrari, D. C. et al. Midbrain dopaminergic neurons generate calcium and sodium currents and release dopamine in the striatum of pups. *Front. Cell Neurosci.* **6**, 7 (2012).
46. Anders, S., Reyes, A. & Huber, W. Detecting differential usage of exons from RNA-seq data. *Genome Res.* https://doi.org/10.1101/gr.133744.111 (2012).
47. Gao, Y., Zhang, J. & Zhao, F. Circular RNA identification based on multiple seed matching. *Brief. Bioinform.* https://doi.org/10.1093/bib/bbx014 (2018).
48. Zhang, X. O. et al. Diverse alternative back-splicing and alternative splicing landscape of circular RNAs. *Genome Res.* https://doi.org/10.1101/gr.202895.115 (2016).
49. Watts, M. E. et al. Circular RNAs arising from synaptic host genes during human neuronal differentiation are modulated by SFPQ RNA-binding protein. *BMC Biol.* **21**, 127 (2023).
50. Lin, W. et al. Foxa1 and Foxa2 function both upstream of and cooperatively with Lmx1a and Lmx1b in a feedforward loop promoting mesodiencephalic dopaminergic neuron development. *Dev. Biol.* **333**, 386–396 (2009).
51. Uhde, C. W., Vives, J., Jaeger, I. & Li, M. Rmst is a novel marker for the mouse ventral mesencephalic floor plate and the anterior dorsal midline cells. *PLoS One* https://doi.org/10.1371/journal.pone.0008641 (2010).
52. Rahimi, K., Venø, M. T., Dupont, D. M. & Kjems, J. Nanopore sequencing of brain-derived full-length circRNAs reveals circRNA-specific exon usage, intron retention and microexons. *Nat. Commun.* **12**, 4825 (2021).
53. Konermann, S. et al. Transcriptome engineering with RNA-targeting type VI-D CRISPR effectors. *Cell* **173**, 665–676.e14 (2018).
54. Anderegg, A. et al. An Lmx1b-miR135a2 regulatory circuit modulates Wnt1/Wnt signaling and determines the size of the midbrain dopaminergic progenitor pool. *PLoS Genet.* **9**, e1003973 (2013).
55. Behrens, S. E. & Luhrmann, R. Immunoaffinity purification of a [U4/U6.U5] tri-snRNP from human cells. *Genes Dev.* **5**, 1439–1452 (1991).
56. Brown, A., Machan, J. T., Hayes, L. & Zervas, M. Molecular organization and timing of Wnt1 expression define cohorts of midbrain dopamine neuron progenitors in vivo. *J. Comp. Neurol.* **519**, 2978–3000 (2011).
57. Izumi, Y. et al. Integrin α5β1 expression on dopaminergic neurons is involved in dopaminergic neurite outgrowth on striatal neurons. *Sci. Rep.* **7**, 1–14 (2017).
58. Diaz-Ruiz, O. et al. Selective deletion of PTEN in dopamine neurons leads to trophic effects and adaptation of striatal medium spiny projecting neurons. *PLoS ONE* **4**, e7027 (2009).
59. Sekine, K. et al. Reelin controls neuronal positioning by promoting cell-matrix adhesion via inside-out activation of integrin α5β1. *Neuron* **76**, 353–369 (2012).
60. Fernández-Chacón, M. et al. iSuRe-Cre is a genetic tool to reliably induce and report Cre-dependent genetic modifications. *Nat. Commun.* https://doi.org/10.1038/s41467-019-10239-4 (2019).
61. Cui, X. et al. Developmental inhibition of long intergenic noncoding RNA, HOTAIRM1, impairs dopamine neuron differentiation and maturation. *Int. J. Mol. Sci.* **22**, 7268 (2021).
62. Dodbele, S., Mutlu, N. & Wilusz, J. E. Best practices to ensure robust investigation of circular RNAs: pitfalls and tips. *EMBO Rep.* **22**, e52072 (2021).
63. Govek, E. E., Newey, S. E. & van Aelst, L. The role of the Rho GTPases in neuronal development. *Genes Dev.* **19**, 1–49 (2005).
64. Bayer, S. A., Wills, K. v., Triarhou, L. C. & Ghetti, B. Time of neuron origin and gradients of neurogenesis in midbrain dopaminergic neurons in the mouse. *Exp Brain Res.* https://doi.org/10.1007/BF00240955 (1995).
65. Bye, C., Thompson, L. & Parish, C. Birth dating of midbrain dopamine neurons identifies A9 enriched tissue for transplantation into parkinsonian mice. *Exp. Neurol.* **236**, 58–68 (2012).
66. Chung, S. et al. Wnt1-lmx1a forms a novel autoregulatory loop and controls midbrain dopaminergic differentiation synergistically with the SHH-FoxA2 pathway. *Cell Stem Cell* **5**, 646 (2009).
67. Adams, K. A., Maida, J. M., Golden, J. A. & Riddle, R. D. The transcription factor Lmx1b maintains Wnt1 expression within the isthmic organizer. *Development* **127**, 1857–1867 (2000).

68. Tang, M. et al. Interactions of Wnt/β-catenin signaling and sonic hedgehog regulate the neurogenesis of ventral midbrain dopamine neurons. *J. Neurosci.* https://doi.org/10.1523/JNEUROSCI.0860-10.2010 (2010).
69. Anderegg, A. & Awatramani, R. Making a mes: a transcription factor-microRNA pair governs the size of the midbrain and the dopaminergic progenitor pool. *Neurogenesis* **2**, e998101 (2015).
70. Lengefeld, J. et al. Cell size is a determinant of stem cell potential during aging. *Sci. Adv.* **7**, 271 (2021).
71. Kwon, C. H. et al. Pten regulates neuronal soma size: A mouse model of Lhermitte-Duclos disease. *Nat. Genet.* https://doi.org/10.1038/ng781 (2001).
72. Hellas, J. A. & Andrew, R. D. Neuronal swelling: a non-osmotic consequence of spreading depolarization. *Neurocrit. Care* **35**, 112–134 (2021).
73. Kosillo, P. et al. Dopamine neuron morphology and output are differentially controlled by mTORC1 and mTORC2. *Elife* **11**, e75398 (2022).
74. van Diepen, M. T. et al. MyosinV controls PTEN function and neuronal cell size. *Nat. Cell Biol.* **11**, 1191–1196 (2009).
75. Switon, K., Kotulska, K., Janusz-Kaminska, A., Zmorzynska, J. & Jaworski, J. Molecular neurobiology of mTOR. *Neuroscience* **341**, 112–153 (2017).
76. Saxton, R. A. & Sabatini, D. M. mTOR signaling in growth, metabolism, and disease. *Cell* **168**, 960–976 (2017).
77. Magri, L. & Galli, R. mTOR signaling in neural stem cells: from basic biology to disease. *Cell Mol. Life Sci.* **70**, 2887–2898 (2013).
78. Kosillo, P. et al. Tsc1-mTORC1 signaling controls striatal dopamine release and cognitive flexibility. *Nat. Commun.* **10**, 1–19 (2019).
79. Marino, S. et al. PTEN is essential for cell migration but not for fate determination and tumourigenesis in the cerebellum. *Development* **129**, 3513–3522 (2002).
80. Nishikawa, S., Goto, S., Yamada, K., Hamasaki, T. & Ushio, Y. Lack of Reelin causes malpositioning of nigral dopaminergic neurons: evidence from comparison of normal and Reln(rl) mutant mice. *J. Comp. Neurol.* **461**, 166–173 (2003).
81. Kang, W.-Y., Kim, S.-S., Cho, S.-K., Kim, S. & Suh-Kim, H. Migratory defect of mesencephalic dopaminergic neurons in developing reeler mice. *Anat. Cell Biol.* **43**, 241–251 (2010).
82. Sharaf, A., Bock, H. H., Spittau, B., Bouché, E. & Krieglstein, K. ApoER2 and VLDLr are required for mediating reelin signalling pathway for normal migration and positioning of mesencephalic dopaminergic neurons. *PLoS ONE* **8**, e71091 (2013).
83. Wang, J., Cai, Y., Lu, H., Zhang, F. & Zheng, J. LncRNA APOA1-AS facilitates proliferation and migration and represses apoptosis of VSMCs through TAF15-mediated SMAD3 mRNA stabilization. *Cell Cycle* **20**, 1642–1652 (2021).
84. Svetoni, F. et al. Post-transcriptional regulation of FUS and EWS protein expression by miR-141 during neural differentiation. *Hum. Mol. Genet.* **26**, 2732–2746 (2017).
85. Fang, L., Ye, T. & An, Y. Circular RNA FOXP1 induced by ZNF263 upregulates U2AF2 expression to accelerate renal cell carcinoma tumorigenesis and warburg effect through sponging miR-423-5p. *J. Immunol. Res.* **2021**, 8050993 (2021).
86. Mochizuki, Y. et al. Alternative microexon splicing by RBFOX2 and PTBP1 is associated with metastasis in colorectal cancer. *Int. J. Cancer* **149**, 1787–1800 (2021).
87. Jacko, M. et al. Rbfox splicing factors promote neuronal maturation and axon initial segment assembly. *Neuron* **97**, 853–868.e6 (2018).
88. Schmid, B. et al. Loss of ALS-associated TDP-43 in zebrafish causes muscle degeneration, vascular dysfunction, and reduced motor neuron axon outgrowth. *Proc. Natl Acad. Sci. USA* **110**, 4986–4991 (2013).
89. Chen, X. et al. TDP-43 regulates cancer-associated microRNAs. *Protein Cell* **9**, 848–866 (2018).
90. Hewamaddumal, C. A. A. et al. Tardbpl splicing rescues motor neuron and axonal development in a mutant tardbp zebrafish. *Hum. Mol. Genet* **22**, 2376–2386 (2013).
91. Ochs, M. E., Josephson, M. P. & Lundquist, E. A. The predicted RNA-binding protein ETR-1/CELF1 acts in muscles to regulate neuroblast migration in caenorhabditis elegans. *G3* **10**, 2365–2376 (2020).
92. Zhao, Y. F. et al. Human antigen R-regulated mRNA metabolism promotes the cell motility of migrating mouse neurons. *Development* **147**, dev183509 (2020).
93. Smidt, M. P., von Oerthel, L., Hoekstra, E. J., Schellevis, R. D. & Hoekman, M. F. M. Spatial and temporal lineage analysis of a Pitx3-driven Cre-recombinase knock-in mouse model. *PLoS ONE* **7**, e42641 (2012).
94. Rodríguez, C. I. et al. High-efficiency deleter mice show that FLPe is an alternative to Cre- loxP. *Nat. Genet.* **25**, 139–140. https://doi.org/10.1038/75973 (2000).
95. Doucet-Beaupré, H. et al. Lmx1a and Lmx1b regulate mitochondrial functions and survival of adult midbrain dopaminergic neurons. *Proc. Natl Acad. Sci.* **113**, E4387–E4396 (2016).
96. Saxena, A. et al. Trehalose-enhanced isolation of neuronal subtypes from adult mouse brain. *Biotechniques* https://doi.org/10.2144/0000113878 (2012).
97. Gomes-Duarte, A. et al. Enrichment of circular RNA expression deregulation at the transition to recurrent spontaneous seizures in experimental temporal lobe epilepsy. *Front. Genet.* **0**, 33 (2021).
98. Kim, D. et al. TopHat2: accurate alignment of transcriptomes in the presence of insertions, deletions and gene fusions. *Genome Biol.* **14**, 1–13 (2013).
99. Glažar, P., Papavasileiou, P. & Rajewsky, N. circBase: a database for circular RNAs. *RNA* **20**, 1666–1670 (2014).
100. Wu, W., Ji, P. & Zhao, F. CircAtlas: an integrated resource of one million highly accurate circular RNAs from 1070 vertebrate transcriptomes. *Genome Biol.* **21**, 101 (2020).
101. Kan, A. A. et al. Genome-wide microRNA profiling of human temporal lobe epilepsy identifies modulators of the immune response. *Cell Mol. Life Sci.* **69**, 3127–3145 (2012).
102. Dull, T. et al. A third-generation lentivirus vector with a conditional packaging system. *J. Virol.* **72**, 8463–8471 (1998).
103. Morello, F. et al. Frizzled3 controls axonal polarity and intermediate target entry during striatal pathway development. *J. Neurosci.* **35**, 14205 (2015).
104. Gruber, A. R., Lorenz, R., Bernhart, S. H., Neuböck, R. & Hofacker, I. L. The Vienna RNA websuite. *Nucleic Acids Res.* **36**, W70–4 (2008).
105. Mi, H. & Thomas, P. PANTHER pathway: an ontology-based pathway database coupled with data analysis tools. *Methods Mol. Biol.* **563**, 123–140 (2009).
106. Joksimovic, M. et al. Spatiotemporally separable Shh domains in the midbrain define distinct dopaminergic progenitor pools. *Proc. Natl Acad. Sci. USA* https://doi.org/10.1073/pnas.0904285106 (2009).
107. Kolk, S. M. et al. Semaphorin 3F is a bifunctional guidance cue for dopaminergic axons and controls their fasciculation, channeling, rostral growth, and intracortical targeting. *J. Neurosci.* https://doi.org/10.1523/jneurosci.2521-09.2009 (2009).
108. Oo, T. F. & Burke, R. E. The time course of developmental cell death in phenotypically defined dopaminergic neurons of the substantia nigra. *Dev. Brain Res.* https://doi.org/10.1016/S0165-3806(96)00173-3 (1997).

Acknowledgements

The authors acknowledge Luk Parijs, Didier Trono, Rui Benedito, Meng Li and Marten Smidt for their kind gifts of reagents. Furthermore, we thank

Youri Adolfs for experimental help and the Pasterkamp group for constructive feedback during this study. This work was supported by the following grants: the Netherlands Organization for Scientific Research (ALW-VICI 865.14.004 to R.J.P.), European Union's Horizon 2020 Research and Innovation Program under the Marie Skłodowska-Curie Grant Agreement No. 721890 (circRTrain ITN) (to J.K., R.J.P.), EpilepsieNL (to R.J.P.), Stichting Parkinson Fonds (to R.J.P.), NWO Gravitation program BRAINSCAPES: Roadmap from Neurogenetics to Neurobiology (NWO: 024.004.012) (to R.J.P.), Danish Council for Independent Research | Natural Sciences (FNU) (to J.K.).

Author contributions

M.R.T. designed and performed experiments with help of O.G., L.W., R.v.D., A.G.D., M.d.W., L.L.v.d.H, L.M., N.v.K., C.v.d.M. and V.R.V.; K.R. designed and performed ONT sequencing. M.T.V. analysed short-read RNAseq data, ONT sequencing data and performed AS analysis. J.K. provided funding and supervision. M.R.-T. and R.J.P. wrote the manuscript with edits from all authors. R.J.P. acquired funding, designed the initial study and provided supervision.

Competing interests

M.T.V is Co-Founder of Omiics. There are no other competing interests.

Additional information

Supplementary information The online version contains supplementary material available at https://doi.org/10.1038/s41467-024-51041-1.

Correspondence and requests for materials should be addressed to R. Jeroen Pasterkamp.

Peer review information *Nature Communications* thanks Alessandro Fiorenzano, Nikolay Shirokikh and the other, anonymous, reviewer for their contribution to the peer review of this work. A peer review file is available.